Cryogenic Ball Valve Development

Research, Optimization, Design and Analysis

Carlos Castro Garcia

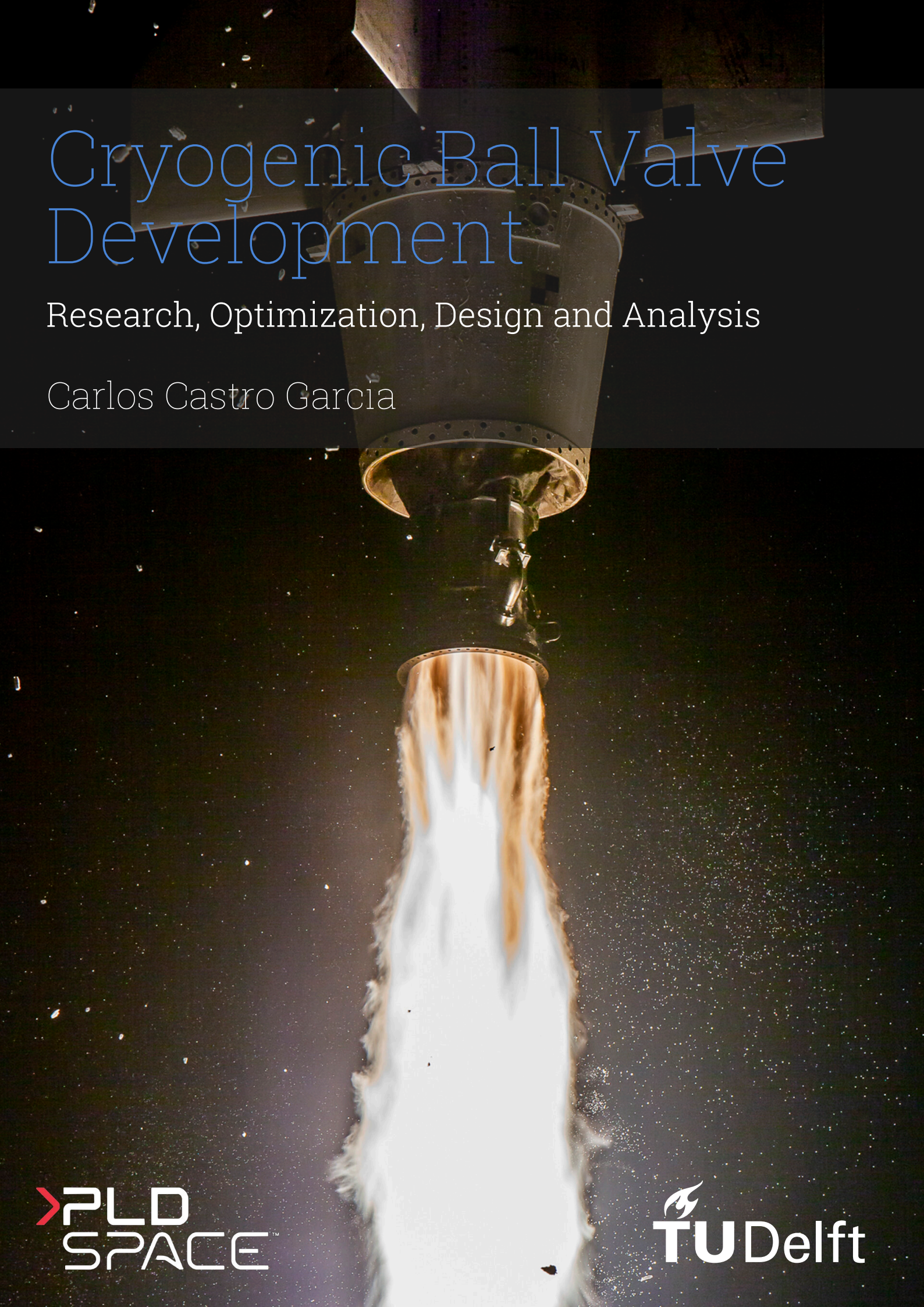

PLD SPACE

TU Delft

Cryogenic Ball Valve Development

Research, Optimization, Design and Analysis

by

Carlos Castro Garcia

to obtain the degree of Master of Science
at the Delft University of Technology,
to be defended publicly on November 11th, 2024 at 13:45h.

Student number:	5003105	
Project duration:	February 2024 – October 2024	
Thesis committee:	Dr. B.V.S. Jyoti,	TU Delft, supervisor
	S. Russell,	PLD Space, supervisor
	Dr. A. Menicucci,	Committee chair
	Dr. ir. E. van Kampen,	External examiner

Cover:	The TEPREL-B engine aboard Miura 1 during its first flight. Picture taken by Manuel Mazzanti
Style:	TU Delft Report Style, with modifications by Daan Zwaneveld

An electronic version of this thesis is available at `http://repository.tudelft.nl/`.

TU Delft

Executive Overview

The main purpose of this thesis project is to design and analyse a ball valve that operates at cryogenic conditions, under a set of defined requirements, parting from a baseline ball valve design provided by the company. Other secondary goals include investigating models as to estimate torque values, estimating flow factor values, and weight optimization.

The structure of the report is as follows. The document opens with a preliminary literature review, which presents the contents of the investigation carried out prior to the research phase of the project. This is followed by a chapter that presents the research questions that will be answered during the technical portion of this document. The torque estimation models are presented in the following chapter, along with a brief validation procedure. The next chapter concerns the estimation of the flow factor of a ball valve, through the usage of the valve's opening area as a function of the ball's rotation. The weight optimization chapter follows, and finally the re-design chapter, where the baseline ball valve design is re-designed using input from the literature review, as well as the weight optimization chapter. The document is closed-off with a chapter compiling recommendations for future work, while explicitly addressing the research questions presented at the beginning of the report. All of these chapters will be elaborated further in the following paragraphs.

The purpose of this chapter is to provide an insight to the reader of the functioning principle of ball valves, as well as some context to the problem that will be tackled in the latter chapters. During this chapter, the requirements for the cryogenic valve are presented, as well as a trade-off justifying the selection of a ball valve for its use within the system. An explanation of how ball valves function follows, along with a presentation of the different design features a ball valve may or may not have.

The next section of this chapter is dedicated to the plethora of ball valves used in heritage rocket propulsion systems. Ball valves from engines such as the SSME, the F-1, or the RL10 are described in detail, noting their operating conditions and their distinct design features. The final section of this chapter reviews some relevant documents found, in regards to ball valve design, torque estimation, and valve analysis. This literature is used to assess the current research gaps within ball valve literature. In order to operate a ball valve, the ball contained within the valve has to be rotated using a certain amount of torque. This torque is often hard to predict, as commercial ball valves usually have torque values provided by the supplier of the valve itself. This chapter aims to present methods by which this torque value can be estimated.

Two separate torque estimation models were found during the literature review. The first model - taken from the Aerospace Fluid Component Designer's Handbook [21] - breaks down torque into two components, the values of which can be found through the implementation of two straightforward equations. The second model - a combination of the model in 'Air-Operated Valve Evaluation Guide' [20] with equations from 'The Optimisation of the Floating Ball Valve Seat Component Design Methodology' [18] - presents a total of 5 separate torque components, which can be used to estimate values for different types of ball valves for both their opening and closing torques, through the different combinations of these 5 components. The implementation of this torque estimation model is considerably harder than that of model 1.

A sensitivity analysis was carried out on both models, which in turn showed that most components in both models are directly proportional to the assigned friction coefficients. This means that during the torque estimation process, friction coefficients must be carefully chosen, and wide ranges should be considered. A variation in the friction coefficient values will inevitably result in considerably different torque values.

In order to validate the results obtained through the usage of these torque estimation models, a validation procedure was carried out, using experimental data of ball valves with a known geometry, under specific operating conditions. From this process, it was found that model 1 is significantly better than model 2 at estimating ball valve torque values when it comes to trunnion ball valves (with an error of 5% or less). Model 2 can also estimate the torque required for floating ball valves, with an error of 8.5% or less. The flow factor can be seen as a way to quantify the 'efficiency' of a component at letting fluid pass through. It is a crucial value in the simulation of the performance of an engine. Although calculating the flow factor of a ball valve fully open is trivial, it can become more difficult to calculate this same value when a ball valve is partially open (or when it is in the process of opening). This chapter presents a methodology by which this value can be calculated as a function of the opening angle of a ball valve.

First, a method is presented by which the opening area of a ball valve can be calculated, at any opening angle. This method was verified by using hand calculations, by comparing area results with values obtained from CAD, and by comparing the results with area of flow of already available ball valves. With the ability to calculate the opening area of the ball valve, the flow rate through the valve can now be estimated.

Flow factor depends on multiple variables. The most critical ones are flow rate (addressed prior) and pressure loss. Calculating pressure loss through a partially open ball valve is non-trivial. As a result, it was decided to estimate a pressure loss distribution (as the valve opens) to calculate the flow factor. This pressure loss approximation was done through the usage of experimental data. With these values now available, the flow factor of a ball valve can be estimated. In accordance with the valve requirements presented in the literature review, the ball valve under consideration must have a mass below a certain value. The baseline ball valve design does not meet this criteria. Therefore, this chapter is dedicated to presenting a methodology by which ball valves can be optimized for weight.

To simplify the problem, only the heaviest component was considered in this exercise - the valve body. It was assumed that this component can be simplified to a hollow cylinder. Considering the inner and outer pressures, the different stress components were calculated, and the most critical stress component was identified. This component defines the thickness of the hollow cylinder (and hence the valve body).

Using the Ashby material selection method, a set of material candidates were selected (by selecting the materials with the highest yield stress-to-density ratio). The mechanical properties of the aforementioned materials were then used to calculate the cylinder thickness required for each material, and approximate their hypothetical weight and cost. This allowed for a final recommendation as to which material is most appropriate for the valve body of the cryogenic ball valve. The baseline design produced internally proved to not be suited to the conditions the ball valve is supposed to work in (cryogenic temperatures and the pressures described in the valve requirements). Because of this, the entire ball valve was re-designed, taking as input the findings of the literature review regarding heritage ball valves that operated under similar conditions. Furthermore, the results from the weight optimization were also implemented, to reduce the valve's weight as much as possible.

One valve was produced per material candidate (a total valve count of 4). These were then subjected to different analysis cases, using ANSYS. These analyses included subjecting the ball valve to the maximum fluid pressure, subjecting it to cryogenic temperatures, and a combined analysis combining both mechanical forces and cryogenic temperatures. The results of these analyses helped in the selection of a suitable material for the valve and the verification of the new ball valve design.

The document is concluded with a chapter compiling all of the findings, and answering the research questions presented at the beginning of the document. Recommendations are made for any future work.

Preface

This thesis project marks the end of my time as a student at TU Delft. After the completion of my bachelor's degree, I embarked on 2-year-long journey within the Space track of the Aerospace Engineering MSc programme. By the end of my first year, I was given the opportunity to join PLD Space, and work in the development of the Miura 5 launcher and its propulsion system. It was within this company where I was given the chance to research the topic of ball valves.

This research project could not have been realized without the help of a multitude of people. I would like to thank my company supervisor, Stephen Russell, who first proposed this research topic during my internship at PLD Space. I would also like to thank my university supervisor, Dr. B.V.S. Jyoti, who guided me along the way. I am most thankful to the Propulsion Analysis team at PLD Space, who helped me with my troubles during the analysis phase of this project. I would also like to thank the Propulsion Testing team, who graciously provided data which I was able to use during my research. Overall, I am thankful to the PLD Space team, who welcomed me with open arms.

To close off this preface, I would like to thank everyone in my life who has supported me through my academic journey. I would like to thank my family for their endless patience, my partner for her relentless support, and my friends for helping me become the engineer I am today. I would have never made it this far without them.

Carlos Castro Garcia
Delft, October 2024

Contents

List of Figures

List of Tables

Nomenclature

Abbreviations

Abbreviation	Definition
ANSYS	Analysis System
CAD	Computer-Aided-Design
CFD	Computational Fluid Dynamics
DBB	Double Block & Bleed
DIB	Double Isolate & Bleed
DPE	Double Piston Effect
FEA	Finite Element Analysis
GN2	Gaseous Nitrogen
HTF	Hydrodynamic Torque Factor
ICBM	Inter-Continental Ballistic Missile
ISA	International Standard Atmosphere
LH2	Liquid Hydrogen
LMAE	Lunar Module Ascent Engine
LMDE	Lunar Module Descent Engine
LNG	Liquefied Natural Gas
LOX	Liquid Oxygen
MFV	Main Fuel Valve
MOV	Main Oxidizer Valve
PEEK	Polyether ether ketone
POV	Preburner Oxidizer Valve
PSI	Pounds-Per-Square-Inch
PTFE	Teflon
RPL	Rated Power Level
SG	Specific Gravity
SSME	Space Shuttle Main Engine
SPE	Single Piston Effect
SPS	Service Propulsion System
UDMH	Unsymmetrical Dimethylhydrazine

Symbols

Symbol	Definition	Unit
A	Area of flow	[m^2]
a_1	Contact half-width from pressure-load application	[in]
a_2	Contact half-width from preload application	[in]
a_3	Contact helf-width from combined load application	[in]
C_v	Flow coefficient	[-]
d	Bore diameter	[in]
d	Moment arm	[in]
d_B	Ball diameter	[in]
d_i	Inner cylinder diameter	[m]
d_{MS}	Mean seat diameter	[in]
d_P	Port diameter	[in]

Symbol	Definition	Unit
d_S	Shaft diameter	[in]
E	Young's modulus	[psi]
$E*$	Reduced Young's modulus	[psi]
F	Seat load	[lb-f]
F_{PL}	Packing load	[lb]
F_{SS}	Sealing load	[lb]
G_{stress}	Gland stress	[psi]
H_P	Packing height	[in]
HTF	Hydrodynamic Torque Factor	[-]
k	Hoop stress constant	[??]
K_v	Flow factor	[m^3/h]
L	Cylinder length	[m]
m	Cylinder mass	[kg]
$\dot{m}$	Mass flow	[kg/s]
P_1	Load per unit length from pressure load	[lb-in^{-1}]
P_3	Combined load per unit lengths	[psi]
p_{01}	Maximum contact pressure under pressure load	[psi]
p_{03}	Maximum contact pressure under combined load	[psi]
P_e	Effective contact pressure from preload	[psi]
P_{in}	Inner cylinder pressure	[Pa]
p_{ls}	Liquid sealing contact pressure	[psi]
P_{out}	Outer cylinder pressure	[Pa]
Q	Flow rate	[m^3/h]
Q_{MAX}	Maximum design flow rate	[gpm]
R	Radius of ball	[in]
R	Cylinder radius at which stress is calculated	[m]
r	Radius of bore	[m]
R_{in}	Inner cylinder radius	[m]
R_{out}	Outer cylinder radius	[m]
r_{out}	Radius of ball	[m]
r_1	Radius of circle 1	[m]
r_2	Radius of circle 2	[m]
SG	Specific gravity	[-]
t	Cylinder thickness	[m]
T_B	Bearing torque	[ft-lb]
T_P	Packing load torque	[ft-lb]
T_{SS}	Static seat torque	[ft-lb]
T_{DS}	Dynamic seat torque	[ft-lb]
T_H	Hydrodynamic torque	[ft-lb]
V	Cylinder volume	[m^3]
v	Velocity of flow	[m/s]
w	Spring load	[N/mm]
α	Seat angle	[rad]
α	Angle between circle intersection and centerline	[º]
α_1	Angle between circle intersection and centerline	[º]
α_2	Angle between circle intersection and centerline	[º]
γ	Ball opening angle	[º]
Δp	Pressure loss	[psi]
θ	Angle between circle intersections	[º]
μ_B	Bearing friction coefficient	[-]
μ_P	Packing friction coefficient	[-]
μ_S	Sealing friction coefficient	[-]
μ_{SS}	Seat friction coefficient	[-]
ρ	Density	[kg/m^3]

Symbol	Definition	Unit
σ_{axial}	Axial cylinder stress	[Pa]
σ_{hoop}	Hoop cylinder stress	[Pa]
σ_{radial}	Radial cylinder stress	[Pa]
τ_B	Bearing friction torque	[in-lbf]
τ_S	Seal friction torque	[in-lbf]
ν	Packing constant	[-]
ν	Poisson's ratio	[-]

1

Introduction

The origins of rocket propulsion date back to the early 20th century, with the research of Konstantin E. Tsiolkovsky into the theoretical aspects of rocket propulsion, and the experiments of Robert H. Goddard, which include the testing of the first liquid propellant rocket [8]. Throughout the 2nd World War and during the post-war period, rocket propulsion development was led by military efforts, particularly of the United States and the USSR. These endeavors resulted in the development of Inter-Continental Ballistic Missiles (such as the Titan II), which allowed for further advancements in the realm of rocket propulsion. Ultimately, it was this technology which allowed for manned spaceflight, and eventually a series of manned Moon landings.

Amongst all of the rocket propulsion systems developed in the past, most of the systems can be classified into the following groups.

- Liquid propellant propulsion
- Solid propellant propulsion

These two types are the most common propulsion systems seen in rockets, although spacecraft in general may be equipped with other types of propulsion systems. Liquid propellant rocket engines are considered to be more efficient and allow for shutdown and throttling, which is why in many launcher systems this propulsion method is chosen. Disadvantages of this system includes the increased complexity (when compared to solid propellant propulsion) and the need of a feeding system, by which propellants are delivered to the combustion chamber(s) of the rocket engine. This second need comes with the necessity of propellant flow control, which implies the presence of valves within said system.

Liquid propellant propulsion systems can generally work with either one propellant (monopropellant) or two propellants (bipropellant). In the latter case, propulsion systems can be designed to work with a variety of propellant combinations. Some of the most common ones are listed below [40].

- Kerosene & Liquid Oxygen
- Methane & Liquid Oxygen
- Liquid Hydrogen & Liquid Oxygen
- Dinitrogen Tetroxide & Monomethylhydrazine
- Dinitrogen Tetroxide & Unsymmetrical Dimethylhydrazine

From these combinations, many of the individual propellants need to be stored in cryogenic conditions, such as liquid oxygen and liquid hydrogen. These, when compared to other propellants that can be stored at room temperature (such as kerosene), can be difficult to handle due to their extremely low temperatures. Furthermore, extra care must be taken when designing components that will be interacting with these fluids. In the context of rocket engines (particularly liquid propellant propulsion systems), valves are a key component. Their main purpose is to regulate the flow of a specific fluid or gas through

a pipe or a duct. Valves are a critical technology in liquid propellant rocket engines, ensuring timely ignition and a safe engine shutdown, amongst other functions.

Ball valves are a specific type of valve which, through the rotation of a ball, can allow or block a fluid (or gas) from flowing from one side of the valve to the other. The ball is equipped with a bore through its center, such that when the ball is at an opening angle of 90º, the ball's bore is aligned with the valve's ports and fluid can pass through the valve. Advantages of this type of valve includes the ability to partially open it (to regulate flow through the valve), and a very low pressure loss when the valve is fully open.

The first ball valve patent dates back to 1871, and was originally designed to overcome the high torques required to operate plug valves (due to elevated temperatures and high contact area). However, at the time the technology did not allow for effective sealing of the fluid contained within the upstream side of the valve. As a result, ball valves remained an untouched subject up until the mid-20th century, where the United States Navy commissioned a study to research valve types more compact and lightweight than the more common gate and globe valves. Another factor contributing to the advancement in popularity of ball valves is the invention of PTFE (Teflon) in the 1930s, as the properties of said material have made it an essential component achieving an effective seal in ball valves [5].

Despite the sparse information regarding ball valve development throughout the 20th century, some of the earliest examples of ball valves usage within rocket engines can be found all throughout the Apollo Program. Engines that use ball valves include the F-1, the AJ10-137, the Lunar Module Descent Engine, and the Lunar Module Ascent Engine. Most of the ball valves found in this program are bi-propellant valves, and usually incorporate redundant mechanisms into their design [2]. Since the end of the space race, ball valves have become more popular. Newer ball valve designs lack the redundancy measures present in older ball valves and are often non bi-propellant. Notable examples of more modern ball valves are the units found in the RL10, LE-7, and RS-25 rocket engines.

PLD Space is considering the usage of a ball valve on their TEPREL-C liquid propellant rocket engine series, to regulate the flow of liquid oxygen. As of now, a baseline design of this ball valve is available, however it has proven to be heavy, unreliable, and not suited for cryogenic conditions. Furthermore, the company lacks knowledge regarding the required torque to operate this valve, and the nature of flow through said ball valve as the valve is opened. As such, the author has been asked to re-design the current cryogenic ball valve, and inquire into the aspects mentioned above.

The main objective of this thesis project is to design and analyse a ball valve that operates at cryogenic conditions, under a set of defined requirements. The secondary objectives of this thesis project are to investigate certain aspects of ball valves, knowledge of which is useful during their design process. These aspects include torque required for operation and the nature of flow as a ball valve gradually opens.

The structure of this document is as follows. Chapter 2 is the chapter that presents the currently available information regarding ball valves - how ball valves work, ball valves used in rocket engines, documentation and relevant literature. Chapter 3 presents the questions to be answered by the end of the research, dividing the required work into discrete work packages. Chapter 4 documents the torque models, their implementation and subsequent validation. Chapter 5 presents a methodology by which the flow factor through a ball valve can be estimated. Next, Chapter 6 which presents a proposed weight optimization process for a ball valve, as well as material selection and verification of the weight optimization results. Finally, Chapter 7, documenting the re-design and analysis process, in order to improve the current ball valve design and to verify the validity of the new ball valve design. The document is concluded with Chapter 8, which compiles the findings of the technical chapters, and answers all of the research questions and subquestions presented in Chapter 3.

As an addendum, four appendices are included at the end of this document. Appendix A presents the Python script of the two torque models discussed during Chapter 4. Appendix B presents the Python script which implements the methodology showcased in Chapter 5. Appendix C contains the

Python script used in Chapter 6 to obtain the results presented in said chapter. Finally, Appendix D, which is the appendix that includes all of the sensitive information that cannot be disclosed in the main document.

2

Literature Review

The role of valves within the aerospace industry is key, especially in launch vehicle technology. Ball valves can provide good performance with relatively low operational torques required. The usage of these types of valves in launch vehicles has been documented throughout the last century, and there is a substantial amount of research regarding industrial ball valves.

The aim of this chapter is to introduce the reader to the valve requirements imposed by the system, ball valve basics, document the state-of-the-art when it comes to rocket engine ball valves, and identify research gaps in the literature & documentation.

The chapter is structured as follows. Section 2.1 presents the high level valve requirements for the relevant system. Section 2.2 presents a trade-off between the most common valve types. Section 2.3 discusses the general operation of ball valves and their different design aspects. Section 2.4 presents ball valves used in various rocket engines, and Section 2.5 briefly presents the literature and documentation found regarding ball valves. Lastly, Section 2.6 documents the findings of this chapter and concludes it.

2.1. High Level Valve Requirements

The system that the valve will be a part of (the rocket engine) imposes a set of constraints and requirements upon the valve's design. These are high level requirements that concern temperature, pressure, and other relevant variables. The requirements are listed in Table 2.1, shown below.

Table 2.1: High Level Requirements for the to-be-designed valve.

Req. ID	Requirement	Keywords
BV.1	The valve shall be able to regulate the flow of Liquid Oxygen.	LOX
BV.2	The valve shall be able to operate at temperatures down to -180 ºC	Cryogenic
BV.3	The valve shall be a normally-closed valve.	Type
BV.4	The valve shall have a mass of no more than 4 kg.	Maximum, mass
BV.5	The valve shall have a port connection size of 2 inches.	Size
BV.6	The valve shall be able to operate at an average pressure of up to x^1 bar.	Pressure, average
BV.7	The valve shall be able to operate at pressures of up to y^1 bar.	Pressure, maximum

BV.8	The valve shall have a minimum flow coefficient (Cv) of z[1] .	Cv, minimum
BV.9	The valve shall be able to operate for at least w[1] cycles.	Operation
BV.10	The valve shall allow for purging of the line.	Purge
BV.11	The valve shall allow for venting of the upstream side.	Cryogenic, venting
BV.12	The valve shall allow for dismantling.	Assembly
BV.13	The valve materials shall be LOX - compatible.	Materials

2.2. Valve Trade-Off

This section presents the justification by which it was decided to use a ball valve to regulate the flow of liquid oxygen to the main combustion chamber. This conclusion is reached after a trade-off, and the reasons as to discard other candidates is shown at the end of this section.

The four main valve designs that will be considered in this trade-off are the ones listed below, along with a brief description of their design.

- **Butterfly Valves:** A type of quarter-turn valve that restricts flow using a rotating disk.
- **Ball Valves:** A type of quarter-turn valve that rotates a ball in order to restrict flow.
- **Globe Valves:** A type of valve that uses linear motion to move a disk into (or out of) the flow as to restrict it.
- **Gate Valves:** A type of valve that inserts a rectangular gate into the flow.

With this brief summary in mind, the following table displays the several advantages and disadvantages of each one of the valve types.

Table 2.2: Trade-off table presenting the advantages and disadvantages of 4 different valve designs [46].

Valve Type	Advantages	Disadvantages
Butterfly Valves	Lightweight and compact Low cost Simple design	Disk is always facing the flow, intrinsic pressure loss Sealing is worse when compared to other valves Choked flow may occur during operation
Ball Valves	Generally reliable Excellent sealing Low pressure drop Low opening times Lightweight and compact Don't require lubricant	Valve seats may be troublesome in cold flow Generally not resistant to high temperatures
Globe Valves	Wear-resistant Low forces to operate High temperature resistance Easy maintenance	High pressure loss compared to other valves Low opening speed Relatively expensive Relatively high mass
Gate Valves	Low forces to operate Low pressure drop Simple design Low cost	Can not be used to regulate flow May generate vibrations during operation High wear than other valves Slow operation Large envelope space needed

[1] Refer to Appendix D for value.

Considering the requirements from Section 2.1, valve type selection can proceed.

Requirement **BV.4** limits the mass of the ball valve to 4 kg or less. In order to comply with this limitation, it is of interest to choose a lightweight valve type. Globe valves are one of the heavier valve types, hence they can be discarded.

Although butterfly valves have a relatively low weight and cost, they have a subpar sealing and a significant pressure loss (as fluid flowing through the valve is partially obstructed by the valve's disk). Hence this valve type can be discarded too.

While not explicitly a requirement, it is beneficial in a rocket engine system to have valves of a compact design, with quick response times - as the timing of start-up sequences are critical to the successful operation of a rocket engine. For this reason, gate valves are also discarded.

With these justifications in mind, the ball valve was selected for a variety of reasons. These include its excellent sealing properties, as well as its low pressure drop and low opening times. Furthermore, ball valves tend to be lightweight and compact. All of these features are considered beneficial within the system.

The full list of justifications as to why a ball valve was selected is shown Table 2.3 below.

Table 2.3: List of the reasons why the butterfly, globe and gate valves were discarded, in favour of the ball valve.

	Justification To Select Ball Valve
Butterfly Valves	• Subpar sealing properties • Significant pressure loss
Globe Valves	• High pressure loss across the valve • Low opening speed • Relatively higher mass
Gate Valves	• Cannot regulate flow of fluid • Generates undesired vibrations • Low opening speed • Non-compact (large envelope needed)

With a valve type selected, the following section is dedicated to the general description of the ball valve.

2.3. Ball Valves Design & Operation

This section documents the different aspects of a ball valve's design, in general terms. Different design options are presented for each one of the valve's design aspects. The operation of a ball valve is also described, to give the reader an idea of how this type of valve functions.

2.3.1. Ball Valve General Description

A ball valve is a component that has as its main function to regulate the flow of a fluid or a gas through itself, by means of rotating a ball. A cross section of an example of a ball valve can be seen in Figure 2.1.

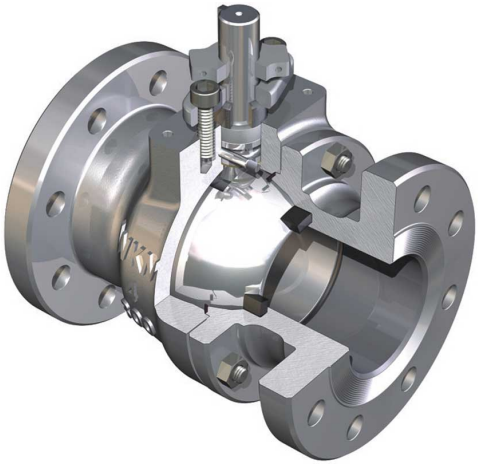

Figure 2.1: Section of a ball valve [10].

In this figure, several features of a ball valve can be appreciated. These will all be discussed later on in this section.

The main component - from which this type of valve draws its name - is the ball. This ball is central to the valve, as it is the component in charge of regulating the flow of the fluid. This ball has a single hole (a bore), as seen in the figure. Depending on the angular position of the ball, this hole may be aligned with the incoming and outgoing ports - allowing fluid flow - or it may be perpendicular to these ports - therefore blocking the flow.

In order to operate (change the angular position of the ball) the valve, the ball is connected to a shaft. This shaft allows the ball to be rotated, either manually or by means of a motor. Nominally, the shaft (and hence the ball) is rotated between 0º and 90º - 0º being the closed position of the ball, and 90º being the fully open position.

To ensure the ball is able to rotate while in operation, and guarantee sealing between the upstream and downstream sides of the valve, ball valves are equipped with seats. These are O-ring-like structures, that are mounted at either side of the valve. These seats are meant to be in contact with the ball's surface at all times, holding it in place. When the valve is closed, these seats help achieve complete sealing.

All of the aforementioned components are encapsulated by what is commonly referred to as the valve's 'body'. This is the structure that forms the upstream and downstream ports, surrounding the ball and holding the seats in place (as shown in Figure 2.1). This structure should be able to withstand every load the valve is subjected to during operation, including the pressure of the fluid and/or gas within the valve, and any thermal stresses.

The operation of a typical ball valve is as follows. In its starting position - where the ball valve has 0º of rotation - the side of the ball completely blocks the valve bore, in contact with the seats which effectively seal the upstream and the downstream sides. At this stage, pressurization of fluid on the upstream side of the valve should not affect the state of the downstream side, due to the ball's position. When the ball is actuated - manually or by a motor - through the shaft, its angular position is gradually changed from 0º up to 90º, and in the process the cross sectional area of the ball's bore gradually increases until said area equals the upstream port area, meaning that the valve is fully open. At this point (90º ball rotation) the ball valve acts as a straight pipe - with relatively low pressure drops across it. This is a significant advantage of using ball valves.

Another advantage of using this type of valves is that it can be partially opened, hence allowing the user to regulate the flow of fluid across the valve. This is done by changing the rotation given to the

ball, which in turn results in a variation of the cross sectional area that the fluid is allowed to flow through. This is a critical feature of this type of valve; it is a main advantage by which it is often selected, when compared to other types of valves.

The purpose of the following subsections is to discuss the different options available regarding every design aspect of a ball valve.

2.3.2. Valve Bore

Ball valves can be separated into two categories: 'full bore' valves and 'reduced bore' valves. Full bore valves have a ball bore diameter equal to that of the port of the valve. This means that across the valve, there is no reduction in the cross sectional area that the fluid can flow through (flow area). An example of this kind of valve is the one shown in Figure 2.1, where it can be seen that the ball's bore has the same diameter as the upstream & downstream ports. This type of ball valve produces a minimal pressure drop when open [13].

In contrast to these types of valves, 'reduced bore' ball valves have a reduction in cross sectional area across the valve. This means that the ball within the valve has a bore diameter smaller than that of the port diameter. An example of this type of valve can be seen in Figure 2.2.

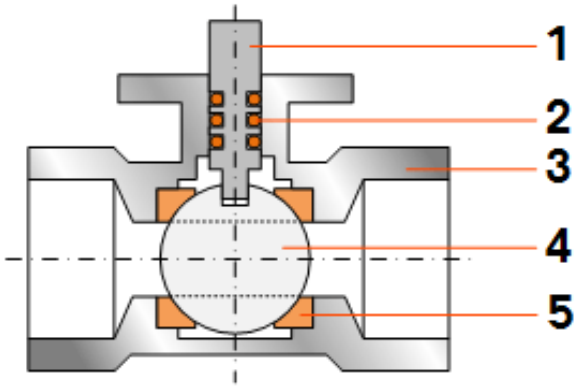

Figure 2.2: Cross section of a reduced bore ball valve [44].

There are several advantages that come with this type of design. The first is that of a more compact valve. Having a reduced bore valve means that overall, the valve will occupy a smaller volume. With this reduction in volume also comes a reduction in weight. Reduced bore ball valves tend to be lighter than their full bore counterparts. Furthermore, reduced bore valves tend to need a smaller torque in order to operate, due to their smaller size [13].

Despite this, reduced bore ball valves also come with a set of disadvantages. The reduction of the cross sectional area of the ball through which fluid can flow results in an increase in the pressure drop across the valve, when compared to an equivalent full bore ball valve. Another disadvantage is that the difference between the port diameter and the bore diameter, which prevents pigging [13].

2.3.3. Valve Port Shape

This subsection presents some of the different inner profiles that the ball of the valve can have.

The most common inner profile is the 'full bore' profile. This means that the opening in the ball is a simple hole, as shown in Figure 2.1. This hole matches the ball valve port diameter, meaning that there is no reduction in cross sectional area across the ball. Another example of a full bore ball can be seen in Figure 2.2, within a reduced bore valve. The benefits of these types of balls is that the pressure drop across the ball remains at a minimum. When the valve is open, the fluid perceives a straight pipe, with no reduction in cross sectional area.

The main disadvantage with these types of valve balls is its transient behavior. As previously mentioned, this ball has an optimal performance when open. However, due to the geometry of the ball, when the valve is in the process of opening the cross sectional area that the fluid can flow through increases non-linearly. This means that regulating the flow of fluid across the valve comes with a higher level of complexity.

There are many other ball designs, but the most popular one is the v-port ball. This design, as shown in Figure 2.3, consists of a ball with a 'v-shaped' hole. The angle of the 'v' is a variable, which directly affects the change in flow as the ball is rotated.

Figure 2.3: Front view of a ball valve, equipped with a V-port ball [26].

The shape of the v-port ball ensures a more linear increase in cross sectional area across the ball as the valve is opened [26].

2.3.4. Ball Mounting Configurations

This subsection discusses the different ways the ball can be mounted unto the body of the valve.

The first method of mounting a ball unto the valve's body is to have it fixed with the stem that actuates the ball. That is, the ball is only held in place by a single structural support (the shaft or stem) and hence its lower side remains unattached to the body. This is called a floating ball valve, and an example of such a valve can be seen in Figure 2.2. On the longitudinal axis (parallel to the flow) the ball is held in place partially by the seat(s) and partially by the stem.

This design feature comes with a set of advantages. First of all, this type of valve is inherently lighter than other options. It is also the simplest design, requiring only a single stem component (and its respective housing) to hold the ball in place and actuate it. Due to this, the manufacture and assembly process is less complicated, and the valve overall has less leak paths - which refers to paths the fluid may take to escape the valve [13].

Despite this, the floating ball valve design also has its downsides. Due to this type of valve only having a single stem, when the valve is pressurized the ball may suffer displacements as a result. Due to the pressure, the ball is pushed against the downstream seat, sealing off the downstream side of the valve from the pressurized upstream. As a result of this, the torque required to operate the valve tends to be higher, as the torque required has to be enough to overcome the friction between the ball and the seat, which directly depends on the pressure applied. This means that operational torques may become significant at elevated pressures [13].

In contrast to floating ball valves, trunnion ball valves have a second, non-actuated stem, as depicted in Figure 2.4. This secondary stem's position is fixed to the valve's body. As a result of this design, when the valve's upstream side is pressurized, the ball remains fixed in place. The trunnion structure increases the valve's overall weight, but since the ball has its position fixed the torque required to operate the valve is usually lower than for floating ball valves [13].

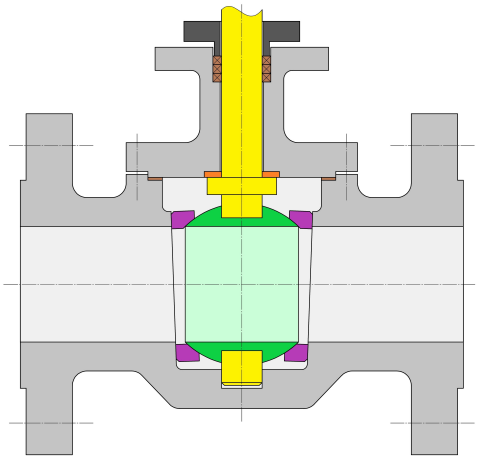

Figure 2.4: Cross section of a trunnion ball valve. The trunnion component is highlighted in yellow, along with the stem [1].

2.3.5. Valve Seats

The seats - as previously described - are ring structures that serve as the interface between the valve body and the ball. They make contact with the ball as to effectively seal the downstream side of the valve from the pressurized upstream side. Seats can be separated into two different categories: 'soft' seats and metal seats.

Soft seats refer to seats made out of thermoplastic or elastomeric materials. These seats often feature seat supports, which hold the seat material in place, acting as the 'casing' of the seat. An example of this type of seat (along with its seat support) can be seen in Figure 2.5, where the material in yellow represents the actual seat, and the metallic material is the seat support. The seat support is equipped with o-rings (represented in black in the image) which are positioned in critical leak path, avoiding potential leaks.

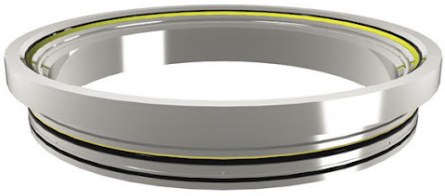

Figure 2.5: A 'soft seat' (in yellow) mounted on a metallic seat support [7].

These types of seats are usually made out of PTFE (Teflon), PEEK, Nylon, and others. These seats may be limited by temperature, but provide good sealing at a relatively cheap price [13].

On the other hand, metal seats can provide an alternate sealing solution. This seating concept consists of direct metal-to-metal contact, between the seat and the ball. These seats are used in extreme conditions, where soft seats would not be appropriate. To improve resistance to wear, contact surfaces are hard faced. In metal seats, sealing may be achieved through the usage of coatings [13].

2.3.6. Valve Body Design

There are four different ways of designing the body of a ball valve. These depend on a variety of factors. The following subsection will be dedicated to explaining these types of valve body designs.

The first design is the 'one piece' body. This design (as its name implies) consists of a body made out of a single piece. It is manufactured as such, and therefore lacks any joints between components. This reduces the number of leaks paths, therefore eliminating the possibility of leaks to the outside of the valve. One-piece designs are usually limited to smaller valves [13].

The second type of valve body to be considered is the 'two-piece' design. This means that the valve body is constructed out of two pieces. An example of this valve is shown in Figure 2.1. These valves (unless welded shut) can be dismantled and maintenance can be carried out [13].

Three-piece ball valve designs have a valve body that consists of three components. An example of this design can be seen in Figure 2.6. Just like the two-piece body design, this design can also be dismantled. In a three-piece valve, the ball is usually housed in the middle piece. This means that maintenance is significantly easier to carry out [13].

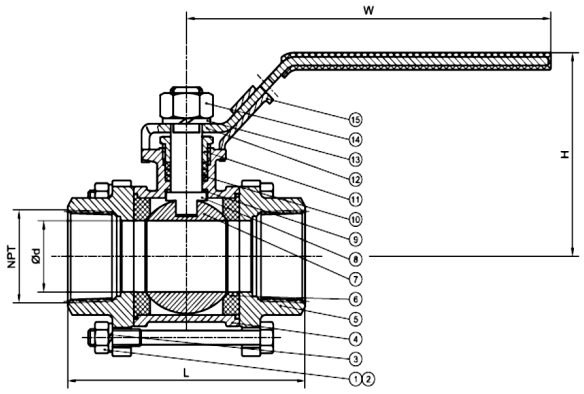

Figure 2.6: Cross section of a three-piece ball valve, manually actuated [22].

Lastly, the 'top entry' body design is discussed. This design can be dismantled, allows access to the inside of the valve via the top side of the valve. The valve does not have to be fully dismantled in order to carry out maintenance. As a matter of fact, maintenance can be carried out in-situ. Due to the nature of this design, these types of valves tend to be heavier than all of the other presented designs [13]. An example of such a valve body can be seen in Figure 2.7.

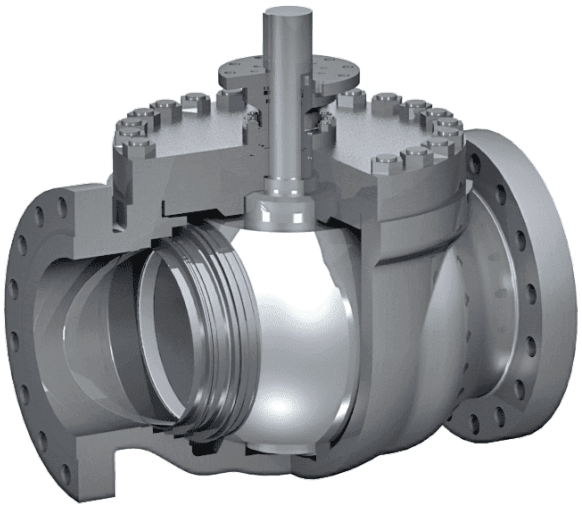

Figure 2.7: A ball valve with a top-entry design, allowing access to the inside of the valve without having to remove the valve from its line [11].

2.3.7. Pressure Relief

During ball valve operation, it is occurrence for fluid to become trapped in the cavity formed between the ball and the valve body (the body cavity). Depending on the type of fluid, evaporation and other effects may cause an abnormal increase in pressure in said cavity. This subsection discusses the different design options meant to avoid or relieve abnormally-high pressures within a ball valve during its operation.

The first important type of seat in the cavity pressure relief process is the 'single piston effect' (SPE). In this design, the seat is pressed unto the surface of the ball via a spring load. As the pressure in the body cavity increases (compared to the pressure within the upstream side of the valve), the seat is pushed away from the ball, relieving the cavity and hence avoiding over-pressure. This effect is referred to as the single piston effect. A single piston effect seat can be designed by changing the geometry of the seat, such that the area facing the body cavity is bigger than the seat's area facing the port of the valve [13].

The second relevant type of ball valve seat is the 'double piston effect' (DPE) seat. With this design, over-pressure from either the upstream section, the downstream section, or the body cavity result in a thrust that pushes the seats against the ball [13]. This means that valves with 2 double piston effect seat rings require a pressure relief device for excess body cavity pressure, as they can not relieve over-pressure through the seats (unlike in SPE).

With these two concepts in mind, two possible ball valve configurations are possible. These are the 'Double Block and Bleed' (DBB) and the 'Double Isolate and Bleed' (DIB). These configurations will be explained below.

In the Double Block and Bleed configuration:

- Both valve seats are single piston effect.
- Medium cavity pressure allows for bleed to either upstream or downstream side.
- Blocks fluid flow from upstream or downstream with medium pressure into body cavity.

This configuration (in theory) does not require a mechanism to relieve body cavity pressure. Pressure within this cavity can be relieved to either the upstream or the downstream side, as the increase in body cavity pressure (relative to either side) results in the seat moving away from the ball's surface, relieving the cavity's pressure [29].

For the Double Isolate and Bleed configuration [29]:

- Either one or both seats are double piston effect (DPE) seats.
- Medium cavity pressure must be relieved via external pressure relief valves, as it is not allowed to flow out of the cavity (as a result of using DPE seats).
- Blocks flow in all directions, unlike the Double Block and Bleed configuration, which allows for leaking from the cavity.
- If upstream seat fails, no leakage downstream occurs thanks to the downstream seat.

Both of these configurations are portrayed in nominal operation in Figure 2.8, where the ball valves are both in the closed position, and the upstream side of the valve is pressurized.

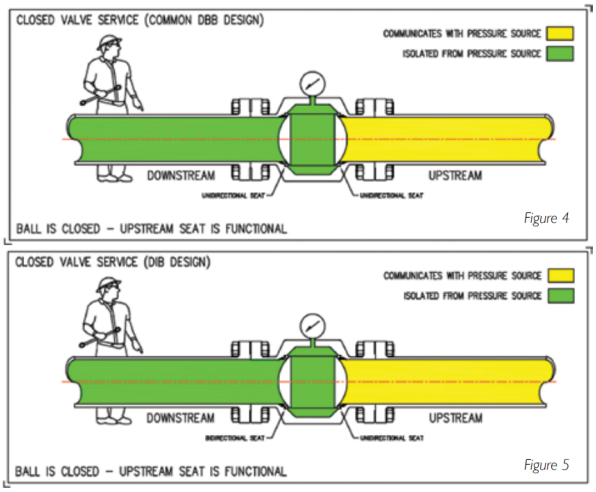

Figure 2.8: Diagram portraying nominal operation of DBB and DIB ball valves, where both seats are operational [29].

Figure 2.9 shows the same case two configurations as in the previous figure, with the difference being that the upstream valve seat has failed and is leaking.

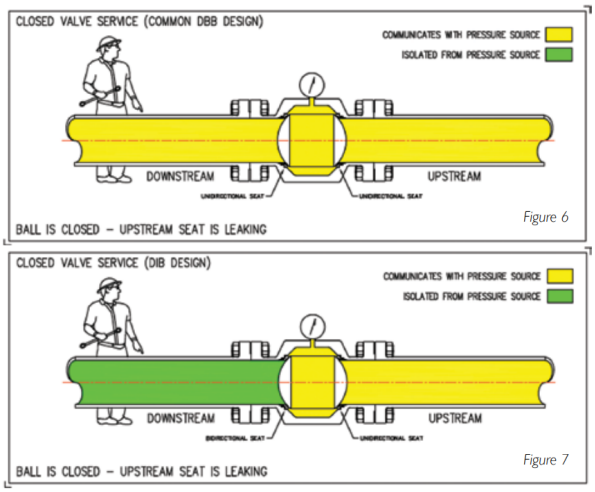

Figure 2.9: Diagram portraying upstream seat failure during operation of DBB and DIB ball valves. Note that DBB fails to isolate the upstream and downstream sides, while DBB can [29].

From the figure, it can be seen that in this situation, the DBB valve leaks all the way to the downstream side of the valve. This is because SPE seats will separate from the ball if they perceive high(er) pressures from the body cavity. Since it is assumed that the upstream seat has failed, the body cavity pressure will be equal to the upstream pressure. This will result in the functional seat allowing flow from the body cavity downstream.

Unlike in the DBB configuration, the DIB configuration succeeds in sealing the downstream side from the upstream, despite having a malfunctioning upstream seat. Once again, due to the failing upstream seat, the body cavity is pressurized. However, the downstream seat does not allow for leakage to the downstream side due to the fact that it is a DPE seat. This means that when there is a pressure difference across the seat (no matter which direction) the seat will be pressed against the ball, ensuring sealing. Despite failure of one of its seats, the DBB valves can still effectively isolate the downstream side from the upstream [29].

2.4. Ball Valves in the Aerospace Industry

The following section documents the various examples of ball valves used in heritage launch vehicles. This includes any and all types of ball valves previously discussed, under any conditions (cryogenic or otherwise).

2.4.1. Space Shuttle Main Engine: Main Oxidiser Valve & Main Fuel Valve

The Space Shuttle Main Engine (SSME), also known as the RS-25, was equipped with a set of two ball valves in order to regulate oxidiser and fuel flow. The designs of these valves were similar, and will be discussed below.

Figure 2.10 depicts a cross section of the Main Oxidiser Valve (MOV) of the RS-25 rocket engine. The working fluid of this valve is cryogenic liquid oxygen (LOX). The MOV is a trunnion ball valve with an inner bore diameter of 2.5 inches, which operates at approximately 278 bar (4040 psia) at 104% of Rated Power Level (RPL) [34]. The body of the MOV is made mainly out of Inconel 718, a high-strength nickel alloy [9].

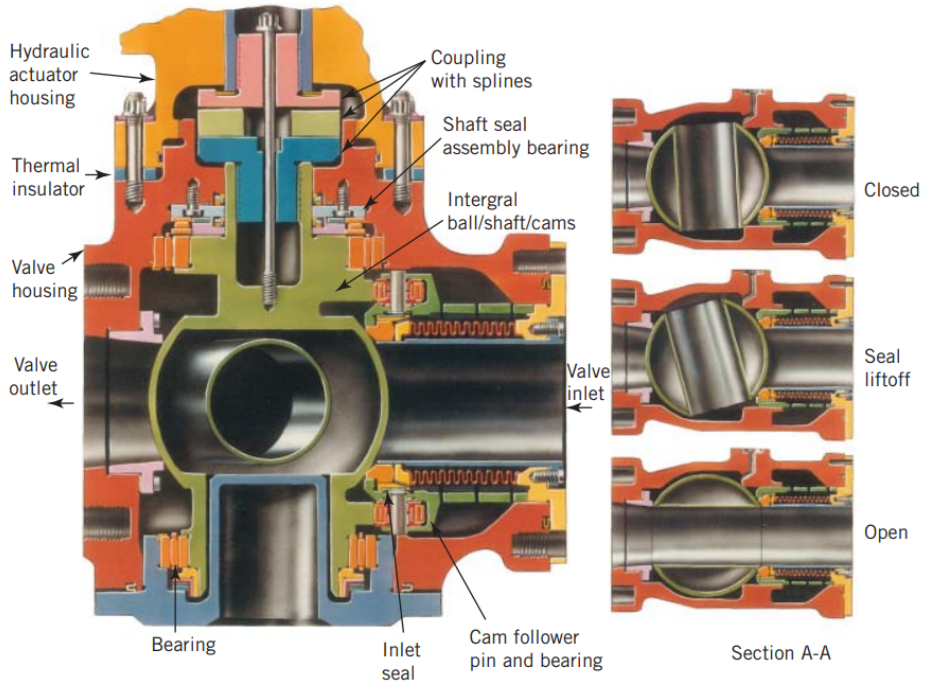

Figure 2.10: Cross section of the Main Oxidizer Valve of the Space Shuttle Main Engine (SSME) [43].

It is noticeable from the diagram that the MOV was equipped with bellows on the upstream seat. Due to the trunnion configuration, these bellows help achieve sealing by exerting a force on the seat, which is consequently pushed unto the ball's surface.

Another remark of this design is that the ball is integrated with the shaft, at least partially. the ball is not a spherical, separate component, and instead protrudes upwards, where it attaches to the couplings, that interface with the hydraulic actuator that operates the valve. This is commonly referred to as an integral ball and shaft [9].

The MOV has a mechanism integrated such that the seat in contact with the valve ball is lifted off of the ball's surface during the first six degrees of operation, easing valve operation [9].

The Main Fuel Valve (MFV) is the second ball valve present within the RS-25. Its design resembles that of the previously described MOV. The RS-25 uses cryogenic Liquid Hydrogen (LH2) as its fuel, which is therefore the working fluid of the MFV. At the inlet, the valve experiences approximately 410

bar (5956 psia) [34].

There are several differences between the MFV and the MOV. Due to the higher pressures experienced by the MFV the body of the valve is made out of a titanium alloy. Said titanium alloy has better performance at cryogenic conditions. In order to achieve a more thorough chilldown of the valve prior to operation, the MFV was turned around, leaving the bellow-seated seals on the downstream side of the ball. Another major difference is the temperatures at which the MFV and the MOV operate. The MFV operates 100 ºR cooler than the MOV, which requires insulation of the outer part of the valve housing. This was done to avoid formations of liquid nitrogen on the surface of the valve [9].

2.4.2. F-1 Engine: Gas Generator Oxidiser & Fuel Valve

During research, it was found that the F-1 rocket engine was equipped with a single ball valve that regulated both fuel and oxidiser flow to the engine's gas generator. This valve was hydraulically operated, where both sides of the valve (the oxidiser and the fuel) were connected to the same shaft. The valve is shown in the gas generator assembly in Figure 2.11, and a cross section of the ball valve is shown in Figure 2.12.

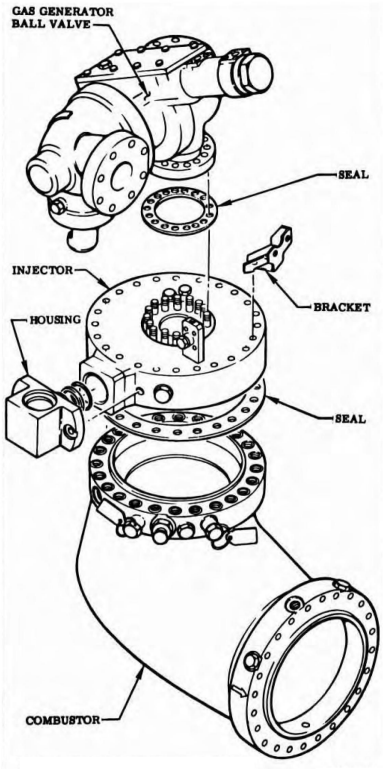

Figure 2.11: Gas generator assembly of Rocketdyne's F-1 rocket engine, showing the bipropellant ball valve [31].

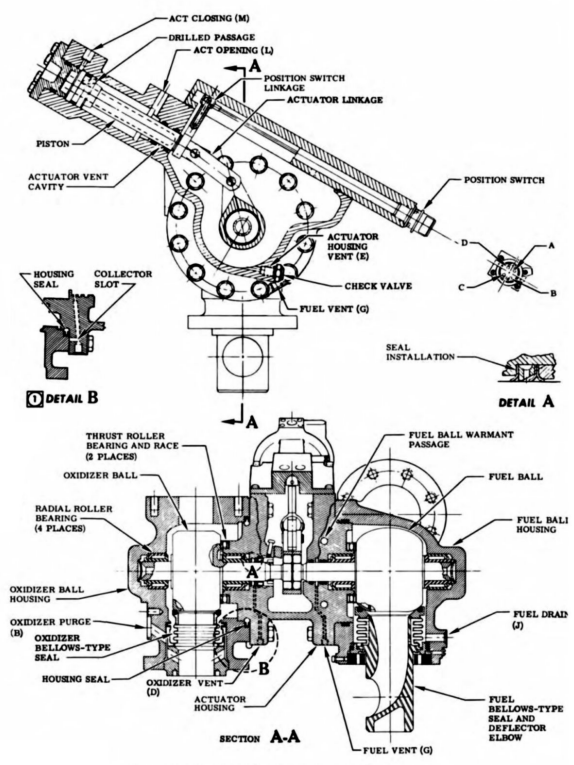

Figure 2.12: Cross section of the gas generator bipropellant ball valve of the F-1 rocket engine [31].

In the figure, it can be seen that the fuel and the oxidiser have separate valve balls to regulate flow. Both of these balls have seats equipped with bellows. It is worthy to note that this valve is technically a trunnion ball valve, as the valve balls are fixed in place by the same shaft, and each ball has a 'secondary' shaft, each attached to a radial bearing.

Due to the (cryogenic) oxidiser and the fuel valves being integrated into one single valve, there was a risk of fuel freezing due to the low temperatures of the adjacent oxidiser. To overcome this, the hydraulic fluid was re-circulated through a warmant passage within the valve body, to prevent freezing of the fuel.

Another notable aspect of the gas generator ball valve is that in the oxidiser side, the inlet and the outlet are opposite to each other (as seen in conventional ball valves such as the one shown in Fig-

ure 2.1). However, when looking at the fuel side, the inlet and the outlet are at an angle of 150º to each other. Although sometimes ball valve designs at right angles can be found, this 150º angle between the inlet and outlet of the fuel section makes this valve an even more peculiar design.

2.4.3. RL10 Engine: Oxidiser & Fuel Pump Inlet Shut-Off Valves

The RL10 rocket engine is equipped with two separate ball valves. These are the Oxidiser Pump Inlet Shut-Off valve and the Fuel Pump Inlet Shut-Off valve, and will be discussed below.

Both of these valves are located just before their respective pumps (the oxidiser and the fuel pumps), therefore both valves operate at low pressure values. They are both spring-loaded valves. The Fuel Inlet Shut-Off valve has a diameter of 3.2 inches (81.28 mm), while the Oxidizer Inlet Shut-Off valve has a diameter of 4.6 inches (116.84 mm), and they weight 13 lb (5.90 kg) and 15 lb (6.81 kg) respectively (both including the operating mechanism) [12]. Schematics for both valves can be seen in Figure 2.13.

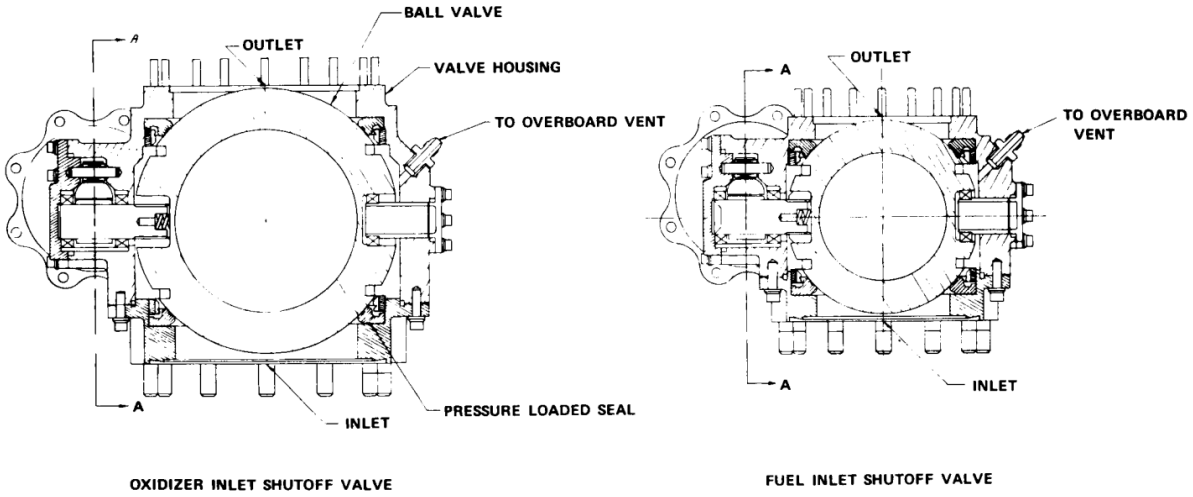

Figure 2.13: Cross sections of both the Oxidizer Inlet Shut-Off Valve (left) and the Fuel Inlet Shut-Off Valve (right) from the RL10 rocket engine. These valves were positioned prior to their respective pumps' inlets [12].

As shown in the figure, both valves are trunnion types. According to the description of these valves, the fluorocarbon rubber seats are spring-loaded - the seats are pushed into the ball's surface via springs. The body cavity of these valves is equipped with a vent port, as seen in the figure. This is to relieve pressure increases within this cavity.

The body, ball, and actuation mechanism housing of the valve are all made out of aluminum, to minimize weight of the system. The rest of the components are made out of stainless steel. Both valves are shown in the picture on Figure 2.14

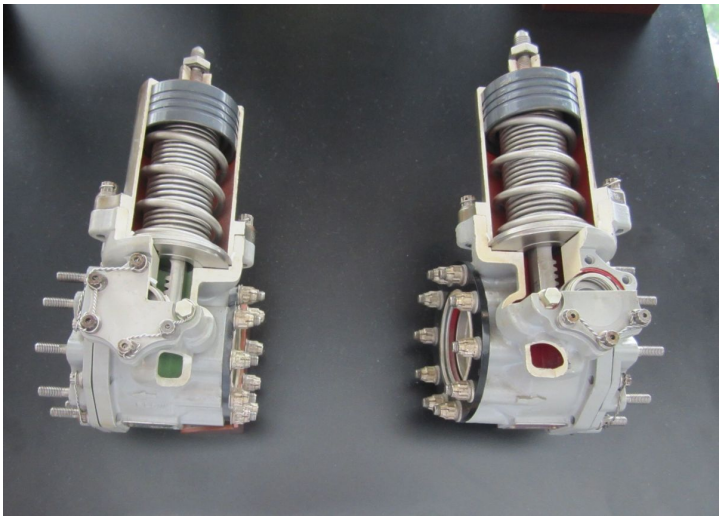

Figure 2.14: The RL10 rocket engine's Oxidizer Inlet Shut-Off Valve (left) and the Fuel Inlet Shut-Off Valve (right) [33].

2.4.4. LE-7 Engine: Main Oxidiser Valve, Main Fuel Valve, Preburner Oxidiser Valve

The LE-7 is a Japanese Liquid Hydrogen - Liquid Oxygen rocket engine. It is equipped with three ball valves: the Main Oxidizer Valve (MOV), the Main Fuel Valve (MFV), and the Preburner Oxidizer Valve (POV). The MOV is located at the exit of the LOX turbopump. Similarly, the MFV is located at the exit of the LH2 turbopump. The POV is located right before the entrance to the preburner, on the oxidizer line [38].

It is known that the MOV and the MFV designs were similar. Both valves are trunnion valves, both actuated via helium gas, in a similar fashion as the valves discussed in Section 2.4.3. The mounting of the actuator to the valve body is different, but it is believed that the working principle of actuation is the same as the RL10 inlet shut-off valves. The LE-7 MOV/MFV valve is shown in Figure 2.15.

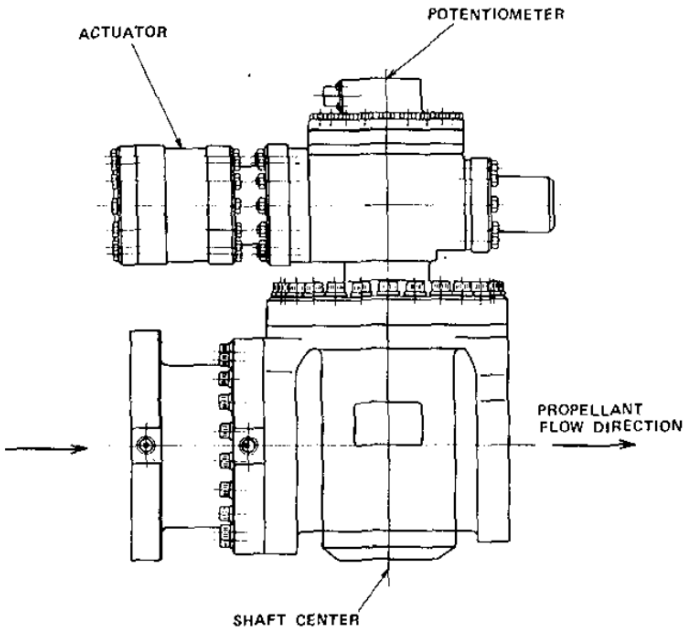

Figure 2.15: Side view of the LE-7 rocket engine's main valve design of which the MOV and the MFV ball valves are based on [25].

Valve operation was tested at 90 bar using liquid nitrogen and liquid hydrogen, to test smooth actuation of the ball. Other tests were also carried out to verify durability of said valves. Under nominal engine conditions, these valves will be subjected to significantly more pressure. Specifically, the MOV will be subjected to 175 bar of pressure on its upstream side, and the MFV will be subjected to 270 bar on its upstream side. It is also expected that the POV will be pressurized to 259 bar [17]. All of these valves are supposed to have similar designs (as the one shown in Figure 2.15), however no more information could be found regarding the differences in design between each individual valve.

2.4.5. Lunar Module Ascent Engine: Oxidiser & Fuel Shut-Off Valves

The Lunar Module Ascent Engine (LMAE) was a rocket engine that used hydrazine (N_2H_4) mixed with unsymmetrical dimethylhydrazine (UDMH) as fuel, and nitrogen tetroxide (N_2O_4) as oxidizer [42]. It was equipped with a single 'Bipropellant Valve Package' that regulated flow of both fuel and oxidizer to the combustion chamber. This package contained 4 individual bipropellant valves, for redundancy. All of the 8 valve balls were meant to be operated simultaneously, by actuation fluid, which allowed into the actuation mechanism via solenoid valves. A schematic of the bipropellant valve package can be seen in Figure 2.16.

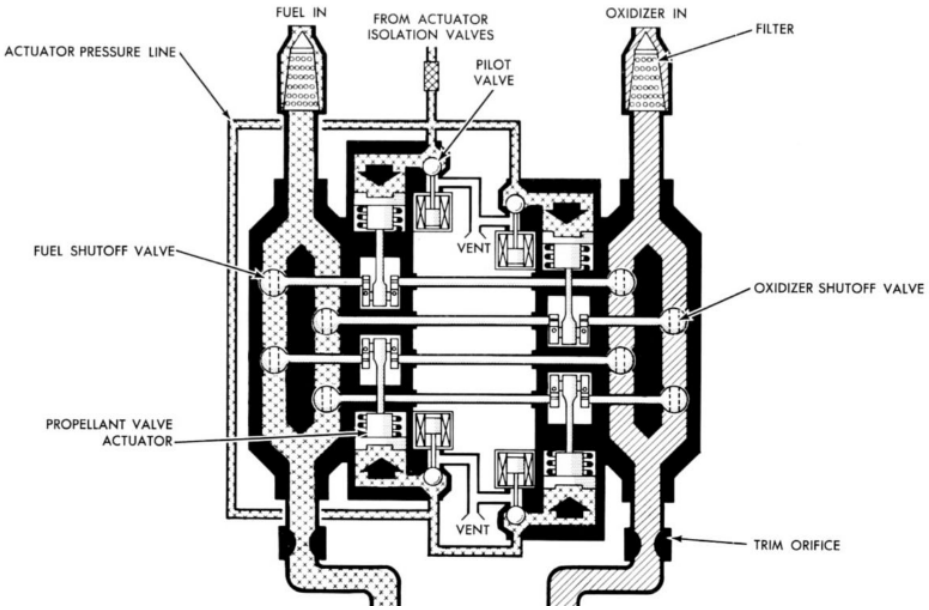

Figure 2.16: Schematic of the configuration of the Lunar Module Ascent Engine's bipropellant valves [32].

The assembly of valves and actuators portrayed in the schematic can be seen in Figure 2.17

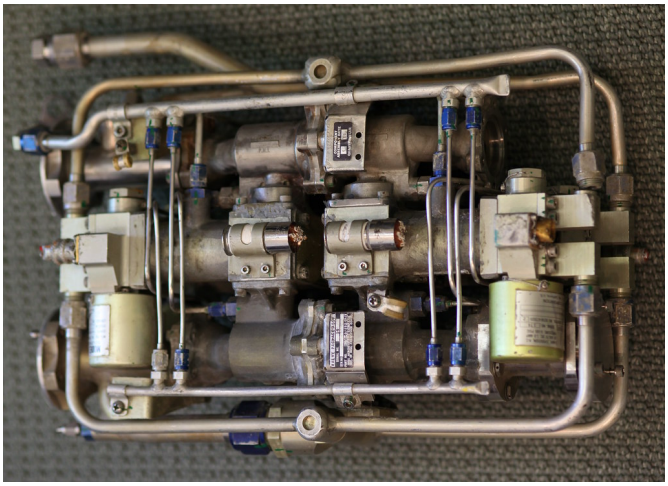

Figure 2.17: The Lunar Module Ascent Engine's Valve Package Assembly [24].

2.4.6. Service Propulsion System Engine: Bipropellant Valves

The Service Propulsion System Engine was a rocket engine that used Aerozine 50 as fuel and nitrogen tetroxide (N_2O_4) as oxidizer [41]. This engine was equipped with a bipropellant valve, of a similar configuration as the one shown in Section 2.4.5, whereby the valve is equipped with two balls per line, and for redundancy there are two lines per propellant (two for the fuel, two for the oxidizer). Having two balls per line provided redundancy for thrust termination at the end of the burn, while having two separate lines for each propellant provided redundancy for the engine's ignition. The valves are all trunnion, pneumatically actuated valves. A diagram of the valve - as well as a flow diagram of the engine - are shown in Figure 2.18.

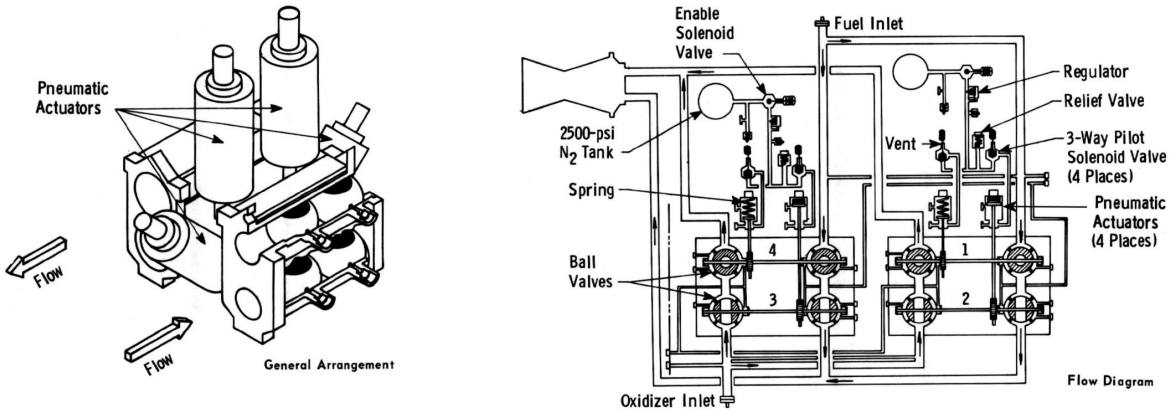

Figure 2.18: Diagram (left) and schematic (right) of the Service Propulsion System Engine's bipropellant valve [41].

The final design of this valve includes a 'one-piece' shaft, that goes through the entire ball. The balls both sit on spring-loaded seats, as shown in Figure 2.19. The valve was operated using pressurized gaseous nitrogen (GN2), in a similar manner as the LMAE valves. For a smoother engine start, the oxidizer ball valves were 8º ahead of the fuel valves, such that when the valve opened the oxidizer would flow first.

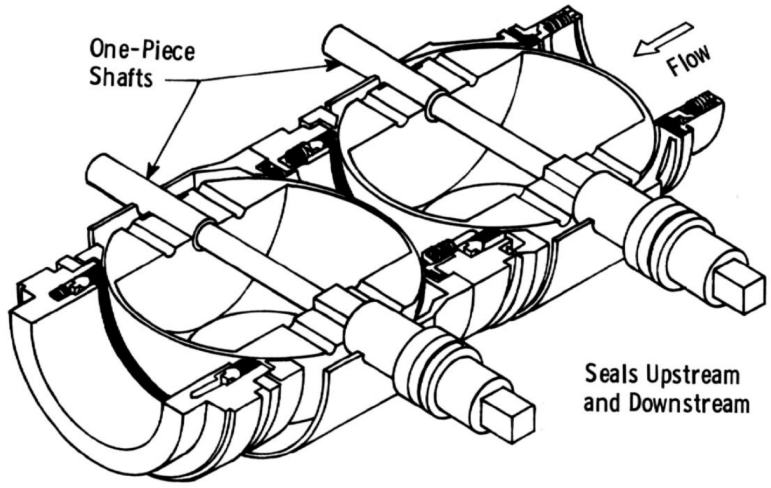

Figure 2.19: Ball design of the bipropellant valve aboard the Service Propulsion System Engine. Note the two-ball, trunnion configuration [41].

2.5. Ball Valves Literature

Following the previously-presented ball valve research and ball valve examples, this section will be presenting the findings from literature relevant to ball valves and their design.

During the literature analysis, a common theme was found between studies and other documentation - the problem of torque estimation. For commercially-available ball valves, the supplier will often provide torque data, so that the user can readily select an actuation method for the valve. Logically, these estimations can not be applied to non-commercial ball valves. There are several sources that attempt to estimate this value using geometric properties of a valve, friction coefficients of seats and other data. An example of this can be found in the ball valves chapter of the Aerospace Fluid Component Designer's Handbook [21]. In the 'Actuation Forces' section, a list of equations to estimate torque is presented. These are presented as 'rules-of-thumb' and provide the following:

- Bearing friction torque, τ_B
- Seal friction torque, τ_S
- Fluid forces

The handbook states that the latter (fluid forces) tend to be small in ball valve units, hence no rule-of-thumb is provided for this component. Furthermore, the handbook states that this rule-of-thumb applies to trunnion ball valves only.

A different paper that attempts to estimate torque is 'The Optimisation of the Floating Ball Valve Seat Component Design Methodology' [18]. Within this document, a set of equations is presented, and it is claimed that these relations can be used to estimate the torque required to operate a ball valve.

- Packing load, T_p
- Static seat torque, T_S
- Dynamic seat torque, T_{DS}
- Hydrodynamic torque, T_H

Equations are provided for 3 out of these 4 components. It is stated that the static seat torque is a value that must be provided by the manufacturer. The author then proposes a static seat torque equation, based on the contact between the ball's surface and the seat. However, this equation relies on the seat having a preload. It is assumed that a valve with seats without a preload are not able to seal. The other torque equations presented in [18] are elaborated on in [20].

In 'Advanced Cryogenic Rocket Engine Program Staged-Combustion Concept', there is a section dedicated to the sizing of a 2" ball valve [6]. Part of this section is dedicated to correlating the required valve opening area to the engine's thrust percentage, as well as correlating said thrust percentage to the dynamic torque required to operate the valve. This is done for different fuel-to-oxidizer ratios and the torque-to-thrust relations obtained are linear (according to Figure 231 [6]).

The aforementioned document also presents information regarding calculations of pressure drops, loss factors (K), and materials selected for the 2" ball valve. More specifically, figure 229 of the technical paper provides a relation between the angular position of a ball valve and the effective opening area of the valve. This is a common topic amongst ball valve literature.

The topic of valve ball angular position to percentage of fluid flow is also tackled by [21], which only shows a 'typical' ball valve opening flow profile, without providing more information. The article 'Design factors for "linear" ball valve: theoretical and experimental studies' details a method which can be used in order to calculate the geometrical opening area of a ball valve as it opens [27]. It must be noted that the geometrical area of flow is not equal to that of the effective area.

An interesting concept proposed by Parker Hannifin in 'Actuation and System Design and Evaluation - OMS Engine Shutoff Valve' is the 'Lifting Ball' design [19]. This design incorporates a mechanism by which, in its closed position the ball seals as in a regular ball valve. The difference comes during operation, whereby the ball is first lifted off the seats of the valve, and once it is lifted off it can be rotated without the ball's surface having to contact the seat. The result of this design is that the amount of torque needed to operate the ball valve is significantly reduced.

The paper 'Design, Manufacture and Simulation of ball valves for oil industrial applications' covers material selection, design and analysis of a ball valve, as well as the manufacture of its constituent parts [4]. This thesis goes into the details of carrying out a Finite Element Analysis (FEA) on the model of a ball valve. The paper itself is concerned with industrial-scale valves, but the methodology followed should be applicable to all ball valve sizes. However, the paper does not detail the effects on the design if the working fluid is at cryogenic temperatures.

The Marquardt Company's technical report 'OMS Engine Shutoff Valve and Actuation System Design and Evaluation' delves into the sizing, design and manufacture of a bipropellant ball valve [47], similar to the one presented in Section 2.4.6. Trivial calculations, such as the sizing of the valve's port, are presented, however the report does not go into detail when it comes to torque estimation or effective flow area estimation. The ball valve designs presented in this technical report all feature a seal lift-off mechanisms, with one of the said designs including a 'solenoid retracted seal'.

'Investigation of the Fluid Flow in a Large Ball Valve Designed for Natural Gas Pipelines' explores the performance and leakage of a DPE design in a trunnion ball valve with metal seats [23]. As indicated by the title of the paper, the analysis is carried out on an industrial-sized ball valve, where the working fluid is methane. Simulations of the valve in operation were carried out, at different opening angles. Through analysis it was determined that the stresses generated in the valve at partially-opened positions make ball valves a less-than-optimal option to regulate flow, limiting ball valves to shut-on / shut-off operations.

The manual 'Liquid Rocket Valve Components' from NASA documents the components of different types of valves [3]. This includes the state-of-the-art for these types of valves, as well as the design criteria for their components. The topics covered by this manual include the following:

- Geometry and Surface Finish
- Seal Retention
- Seat Stress
- Alignment

Within the document, examples of existing valves are given for said topics, and design requirements / criteria are documented as well.

'Liquid Rocket Valve Assemblies' is a NASA manual that contains information on valve selection, heritage valves, and valve design [2]. Although it does not have the same amount of detail as the 'Liquid Rocket Valve Components' manual, it provides a high-level overview of valve selection and design, discussing the state-of-the-art and presenting design criteria for different valve aspects. This document also provides a table listing a number of heritage valves, which includes the type of valve and their operational conditions.

The paper 'Fluid dynamic analysis of liquefied natural gas flow through a cryogenic ball valve in liquefied natural gas receiving stations' contains a simulation of the opening and closing behaviour of a ball valve while in operation [28]. In this paper, the dynamic flow characteristics are found through analysis and compared to experimental measurements. The sole focus of this paper is to analyse the flow of (cryogenic) liquefied natural gas (LNG) from a fluid dynamics perspective, neglecting the structural aspects of the valve.

The research paper 'Transient flow dynamics behaviors during quick shut-off of ball valves in liquid hydrogen pipelines and storage systems' uses a similar approach as the previous paper, to investigate the dynamic behaviour of a ball valve where the working fluid is liquid hydrogen [39].Similarly to the previous paper, this document also focuses more on the fluid dynamics aspect, such as pressure fluctuations and velocity distributions of the flow.

2.6. Conclusions

The beginning of this chapter summarized the high-level requirements for a valve imposed by the system. These requirements impose constraints on the design of the valve. The valve trade-off presented the different advantages and disadvantages of the most common valve designs, which resulted in the selection of the ball valve.

The selection of the ball valve was followed by a study of the operation and design of a typical ball valve, covering the different aspects of a ball valve's design. This was followed by a compilation of ball valve designs present in other rocket engines. This serves as an indication of the most common features of aerospace ball valves.

The last section in this chapter discussed the ball valve literature that was found during research. This includes scientific papers as well as heritage documentation of ball valves. With this section, relevant topics in documentation were identified as well as their respective research gaps. It was noted that there exists few methods to estimate operating torque or flow factor values for non-commercial ball valves.

3

Research Proposal

Having presented the requirements for the ball valve that will be designed, and with the background information presented in Chapter 2, the reader may now have a clearer view on the functioning principles of ball valves, their history, and the current knowledge gaps in scientific literature.

The purpose of this chapter is to briefly present the structure of the research formulated parting from the literature review presented in Chapter 2.

Section 3.1 presents the research objective as well as the research questions that were found after analyzing the ball valve literature and documentation. Section 3.2 presents the work packages which comprise the research phase of the project.

3.1. Research Objective & Questions

The objective of the research is stated below.

- The research objective is to research, design, iterate and analyse a cryogenic ball valve.

Based on the research and literature presented throughout Chapter 2 - having the research objective in mind - a number of research gaps were identified and were subsequently used to draft the following set of research questions. To ease the approach to these research questions, each question has been broken down into sub-questions.

- **RQ1:** How can a ball valve be optimized for weight?
  - **RQ1.a:** Which ball valve components can be mass-optimized?
  - **RQ1.b:** How can the structure of a mass-optimized ball valve be verified?
- **RQ2:** How does fluid flow change as the ball valve is operated?
  - **RQ2.a:** How does opening area change as the ball valve is operated?
  - **RQ2.b:** How does flow factor change as the ball valve is operated?
- **RQ3:** How much torque is required to operate a ball valve?
  - **RQ3.a:** How can a ball valve's operational torque be modelled?
  - **RQ3.b:** How can a ball valve's torque model be validated?
- **RQ4:** How can the current ball valve design be improved?
  - **RQ4.a:** What ball valve elements are required for this specific application?
  - **RQ4.b:** How can said elements be incorporated into the current design?
- **RQ5:** What effects does cryogenic conditions impose on the operation of a ball valve?

  - **RQ5.a:** How do cryogenic conditions affect mechanical properties of the ball valve's components?
  - **RQ5.b:** How do cryogenic conditions affect surface properties of the ball valve's components?
- **RQ6:** How can the conclusions & findings be extrapolated to other ball valves?
  - **RQ6.a:** How do operational conditions differ in other ball valves within the system?
  - **RQ6.b:** What design changes could be implemented as to adapt the current ball valve design to said operational conditions?

3.2. Work Packages

This section contains the different work packages drafted after considering the research questions presented in Section 3.1. The work packages are presented in (roughly) chronological order in the list below.

- **WP1:** Review of current valve design
- **WP2:** Torque estimation model
- **WP3:** Torque model validation
- **WP4:** Geometric area model & verification
- **WP5:** Effective area model
- **WP6:** Structural analysis of current design
- **WP7:** Design iteration(s) & analyses
- **WP8:** Considerations in future valves

Through the completion of these discrete work packages it is aimed to answer all of the research questions and respective subquestions presented in Section 3.1.

3.3. Research Plan

With the list of the identified work packages (shown in Section 3.2), a Gantt chart was drafted to estimate the duration of each task. The Gantt chart was made taking into consideration planned holidays, and the deadline to submit the thesis draft. The Gantt chart is shown below.

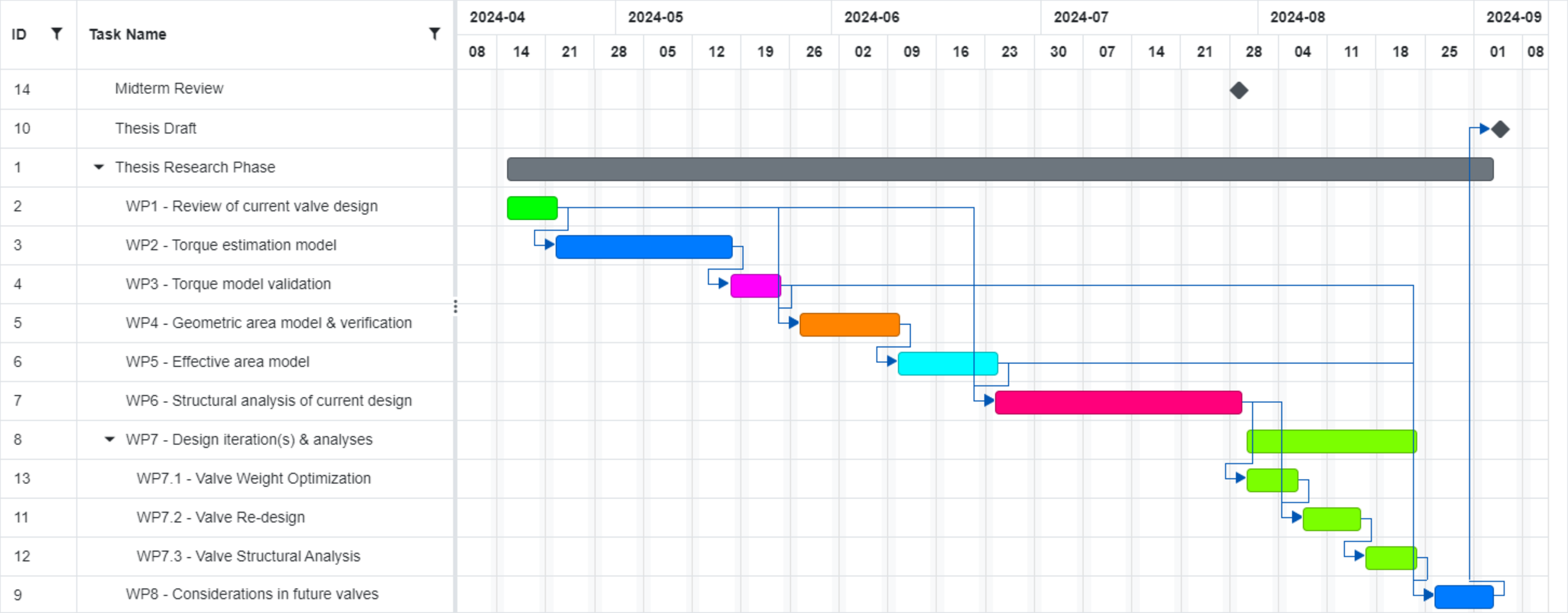

4

Torque Estimation Model

The operating concept of a ball valve is that of rotating one of its key components - the ball - as to either allow or stop fluid flowing through the valve. Predicting the torque required to rotate said ball is an essential task in ball valve design. Knowing the required torque to operate a ball valve aids in the selection of a motor to operate said valve. Most commercially-available ball valves have torque data directly provided by manufacturers. However, only a handful of torque models are available to the public, some of them presented in Section 2.5.

The purpose of this chapter is to present a torque prediction model that can accurately determine the maximum operating torque values for opening and closing a ball valve, as well as validating the model results with experimental data.

This chapter is structured as follows. Section 4.1 discusses the main torque model used, as well as other considered models. This section is followed by Section 4.2, which shows the results of sensitivity analyses for the torque models. This is followed by Section 4.3, where the values obtained from torque models are compared to experimental ball valve data. Section 4.4 concludes the chapter, by summarizing the methods used and the results obtained.

4.1. Torque Models

There are two main models that were considered for torque estimation. Both of these were previously mentioned during the literature review, in Section 2.5. The first model is a set of estimations presented in the Aerospace Fluid Component Designer's Handbook [21]. The second torque estimation procedure is the one presented in 'The Optimisation of the Floating Ball Valve Seat Component Design Methodology' [18], which is itself based on the relations presented in 'Air-Operated Valve Evaluation Guide' [20]. Both of these torque estimation models will be explained and elaborated on in this section.

4.1.1. Torque Estimation Model 1

In the Aerospace Fluid Component Designer's Handbook, the method by which torque is estimated is by deconstructing the total torque required to operate a ball valve into 3 separate components. These are the following:

- Bearing friction torque, τ_B
- Seal friction torque, τ_S
- Fluid forces

The handbook provides rules-of-thumb to estimate the first two values, τ_B and τ_S, while neglecting the fluid forces component, claiming that the later component is usually small in ball valves [21]. The equations by which bearing friction torque and seal friction torque are calculated can be found below.

$$\tau_B = 1.75 \cdot 10^{-3} \cdot \Delta p^{\frac{3}{2}} \cdot d^2 \cdot \mu_b \tag{4.1}$$

$$\tau_S = 0.625 \cdot \Delta p \cdot d^3 \cdot \mu_s \tag{4.2}$$

Where Δp is the pressure differential across the valve (in psi), d is the bore diameter (inches), μ_B is the (dimensionless) friction coefficient of the bearing, and finally μ_S is the (dimensionless) friction coefficient of the valve's seals. Both torque values are given in in-lbf. It is worth to note that these relations only apply to 'fixed' ball valves[21] - referring to a trunnion ball valve configuration. This means that the results from the estimations can not be applied to floating ball valves.

Both expressions directly depend on friction coefficients (apart from other variables set by requirements). These relations are very sensible to changes in friction coefficients, therefore the value of these variables is critical. This issue will be discussed later on in this chapter.

Once the relevant equations were identified, they were implemented into a Python script. In order to verify their implementation, Figure 6.2.3.2k from the handbook was recreated, in Figure 4.1.

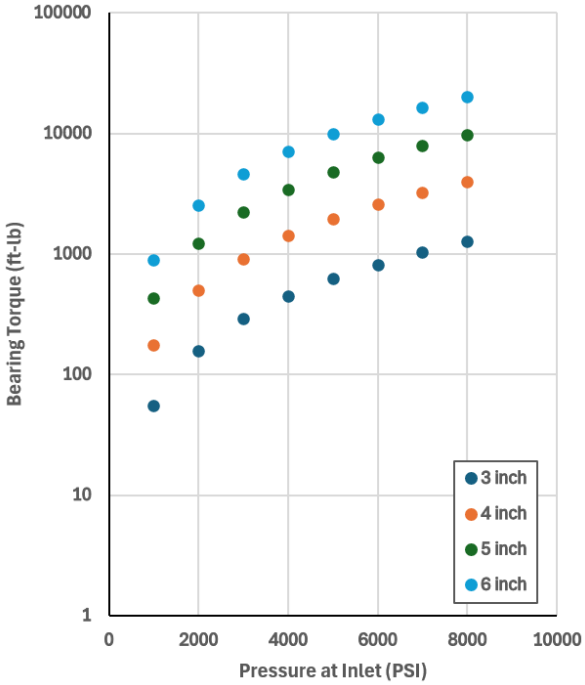

Figure 4.1: Figure from the fluid handbook [21], recreated using an Excel implementation of the torque model presented in Appendix A.

4.1.2. Torque Estimation Model 2

Compared to the first torque estimation model, the second model is significantly more complex. It relies on far more equations, but can give torque estimations for both floating ball valves and trunnion ball valves. Two separate torque values can be obtained, one for the opening of the valve, and one for the closing process.

This estimation method consists of 5 different torque components, all of which are listed below.

- Packing torque, T_P
- Static seat torque, T_{SS}
- Dynamic seat torque, T_{DS}
- Bearing torque, T_B
- Hydrodynamic torque, T_H

The packing torque refers to the torque required to overcome the friction forces generated due to the packing of the ball valve. The static seat torque refers to the torque required to overcome the friction

from the contact of the ball with the valve seats. The dynamic seat torque is the torque experienced by the stem due to the ball as it rotates and experiences friction against the valve seats. The bearing torque is the torque required to overcome the friction forces from the bearing (of the secondary axis, therefore this only applies to trunnion ball valves). Finally, hydrodynamic torque, which is the torque required to overcome the fluid forces as the valve opens.

Through different combinations of these 5 components, this estimation method can give values for maximum required torque for the following cases.

- Floating ball valve, opening: T_P + T_{SS} + T_{DS} + T_H
- Floating ball valve, closing: T_P + T_{SS} + T_{DS}
- Trunnion ball valve, opening: T_P + T_{SS} + T_B + T_H
- Trunnion ball valve, closing: T_P + T_{SS} + T_B

The expressions presented in the 'Air-Operated Valve Evaluation Guide'[20] aim to estimate the values of three of these five components - T_{DS}, T_B and T_H. The equations for these three components are presented below.

$$T_{DS} = \frac{\Delta P \cdot \frac{\pi}{4} \cdot d_{MS}^2 \cdot d_B}{\sqrt{d_B^2 - d_{MS}^2}} \cdot \mu_S \cdot \frac{d_B + \sqrt{d_B^2 - d_{MS}^2}}{48} \tag{4.3}$$

$$T_B = \Delta P \cdot \frac{\pi}{4} \cdot d_{MS}^2 \cdot \mu_B \cdot \frac{d_S}{24} \tag{4.4}$$

$$T_H = \frac{1}{12} \cdot \Delta P \cdot \frac{HTF}{100} \cdot d_P^3 \tag{4.5}$$

Where ΔP refers to pressure difference across the valve (in PSI), d_{MS} refers to the mean seat diameter (in inches), d_B refers to the ball diameter (in inches), μ_S refers to the seat friction coefficient, μ_B refers to the bearing friction coefficient, d_S refers to the shaft diameter (in inches), and d_P to the port diameter (in inches). Note that all of the torque values are given in ft-lb.

Equation (4.5) depends on another variable not seen in the rest of the equations, which is the Hydrodynamic Torque Factor (HTF). To calculate this factor, first the equivalent system resistance (K_{SYS}) must be found. This can be done using the following expression.

$$K_{SYS} = \frac{894.01 \cdot d_P^4 \cdot \Delta P}{Q_{MAX}^2} \cdot \frac{62.4}{\rho} \tag{4.6}$$

Where Q_{MAX} refers to the maximum design flow rate, in gallons-per-minute, and ρ refers to the density of the fluid, in lb/ft^3.

Once the equivalent system resistance is known, the HTF value can be found using the graph shown in Figure 4.2.

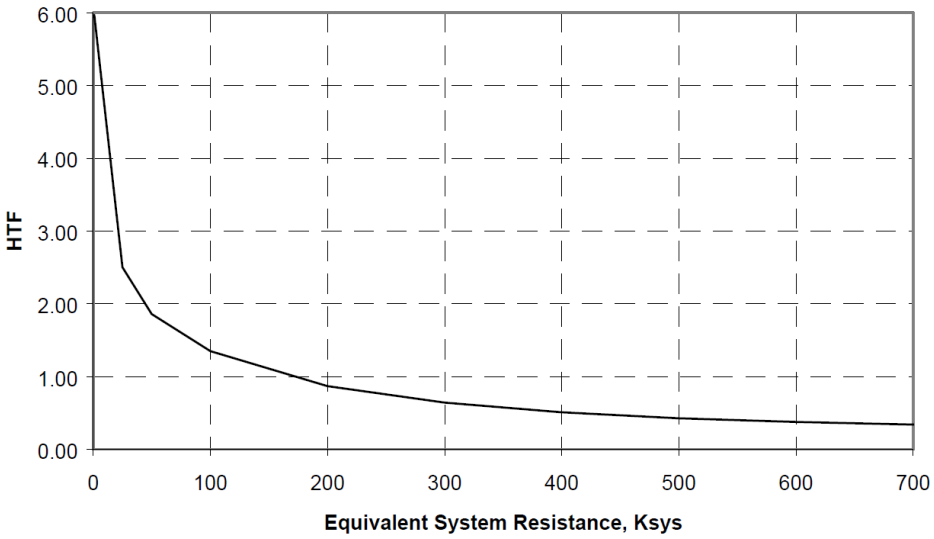

Figure 4.2: Hydrodynamic Torque Factor (HTF) vs. Equivalent System Resistance (K_{sys}) [20].

Once the HTF value is found, it can be plugged back into the hydrodynamic torque equation (shown in Equation (4.5)). The remaining torque components (T_{DS} and T_B) can be found using geometry of the valve, its surface properties, and the valve's operational conditions.

According to the guide[20], the other two components (T_P and T_{SS}) should be obtained from the valve's supplier or from static experimental data. It will be assumed that neither of these are available for the considered valve. As such, there is a need to estimate both of these torque components. The thesis paper 'The Optimisation of the Floating Ball Valve Seat Component Design Methodology'[18] suggests a methodology by which both of these components can be estimated. Furthermore, it provides criteria by which to check whether the ball valve will successfully seal or not. This procedure will be elaborated on below.

The first estimated torque component is the packing torque, T_P. The equation for this value is given below.

$$T_P = F_{PL} \cdot \frac{d_S}{2} \tag{4.7}$$

Where F_{PL} is the packing load, and can be calculated using the following equation.

$$F_{PL} = G_{stress} \cdot \nu \cdot \pi \cdot d_S \cdot H_P \cdot \mu_P \tag{4.8}$$

Where μ_P refers to the packing friction coefficient (usually between 0.1 and 0.2), H_P the height of the packing (in inches), ν is a constant (assumed to have a value of 0.5), and G_{stress} is the gland stress, commonly assumed to be 1.5 times the system design pressure (in PSI).

In order to estimate the value of the static seat torque (T_{SS}), a more complex procedure must be followed. This process is documented below.

The first step to be taken is to calculate whether the valve can achieve sealing in its current state[18]. First, the force that the seat perceives (F_{PL}) due to the applied pressure has to be calculated.

$$F_{PL} = \Delta P \cdot \frac{\pi \cdot d_{MS}^2}{4} \tag{4.9}$$

Parting from this equation, sealing load can be calculated using Equation (4.10).

$$F_{SS} = F_{PL} \cdot cos(\alpha) \tag{4.10}$$

Where α is the angle formed between the center of the ball, the seat (mean seat diameter) and the central axis of the port of the ball. The design contact load can then be calculated using the following equation.

$$P_1 = \frac{F_{SS}}{\pi \cdot d_{MS}} \tag{4.11}$$

P_1 can then be used in the following equation, to calculate the maximum contact pressure.

$$p_{01} = \frac{P_1}{\pi \cdot a_1} \tag{4.12}$$

Where the value of a_1 can be found using Equation (4.13)

$$a_1 = \sqrt[3]{\frac{4 \cdot R \cdot P_1}{\pi \cdot E*}} \tag{4.13}$$

Where R refers to the radius of the ball (d_B / 2), and $E*$ is the reduced Young's modulus, and can be calculated using the following equation.

$$\frac{1}{E*} = \frac{1 - \nu^2}{E} \tag{4.14}$$

Where E is the Young's modulus of the seat material, and ν the Poisson's ratio of the seat material.

Since the medium flowing through the valve is assumed to be a liquid (Liquid Oxygen), the required sealing stress can be determined using the following expression.

$$p_{ls} = 1.05 \cdot \Delta P \tag{4.15}$$

If p_{ls} is smaller than p_{01}, sealing will be achieved in the valve. Usually, this is not the case with valves whose seats lack a spring load (refer to Section 2.3.7). To check if sealing is achieved by adding a spring load, a similar procedure can be followed, bar a few changes.

First, one must know the pre-load caused by the spring load (w, in N/mm). This can then be used to find out the total load:

$$P_3 = P_1 + w \tag{4.16}$$

The value of P_3 can then be plugged in to Equation (4.13), substituting P_1. This will result in a new value, a_3. This value can then be plugged (along with P_3) into Equation (4.12), to obtain p_{03}. This is the maximum contact pressure under the combined load (the pressure from LOX and spring load). If this value is larger than the previously-calculated p_{ls}, the valve is considered to be sealing. This functionality is implemented into the written Python script, to inform the user whether the valve being considered actually seals or not.

Once sealing has been verified through the method described above, the static seat torque can be calculated. The first step in this process is to find out the value of a_2, which can be found by using Equation (4.13) and substituting P_1 with w.

Next, P_e can be calculated similarly, by plugging in a_2 and w into Equation (4.12), substituting a_1 and P_1 respectively. Using the obtained values, the seat load (F) can be calculated using the equation presented below.

$$F = 2 \cdot \mu \cdot P_e \cdot (2 \cdot a_2) \cdot \pi \cdot d_{MS} \tag{4.17}$$

To calculate the torque due to this force, F must be multiplied by the moment arm. The moment arm can be calculated from geometry as follows.

$$d = \sqrt{d_B^2 - d_{MS}^2} \tag{4.18}$$

And finally, the static seat torque is given by Equation (4.19).

$$T_{SS} = F \cdot d \tag{4.19}$$

Similarly to the first model presented in Section 4.1.1, this model's static seat torque (as well as other torque components) heavily depends on the friction coefficient(s) assigned.

4.2. Torque Models Sensitivity Analysis

During the drafting of the Python script where the torque models were implemented, it was observed that the output (torque values) depend heavily on the friction coefficients used as input. For this reason, it was decided to do a sensitivity analysis on the Python functions. The purpose of this section is to document the sensitivity analysis process.

4.2.1. Torque Estimation Model 1 Analysis

As discussed in Section 4.1.1, this model is composed of 2 separate components - bearing and seal friction torques (μ_B and μ_S respectively).

Equation (4.1) shows that the bearing torque is directly proportional to the friction coefficient. The same, proportional relation can be seen in the sealing torque equation, in Equation (4.2).

To help visualize these, a graph was plotted showing the variation in both of these torque components, as the friction coefficient is changed. Furthermore, the sum of their components was also plotted. This is shown in Figure 4.3

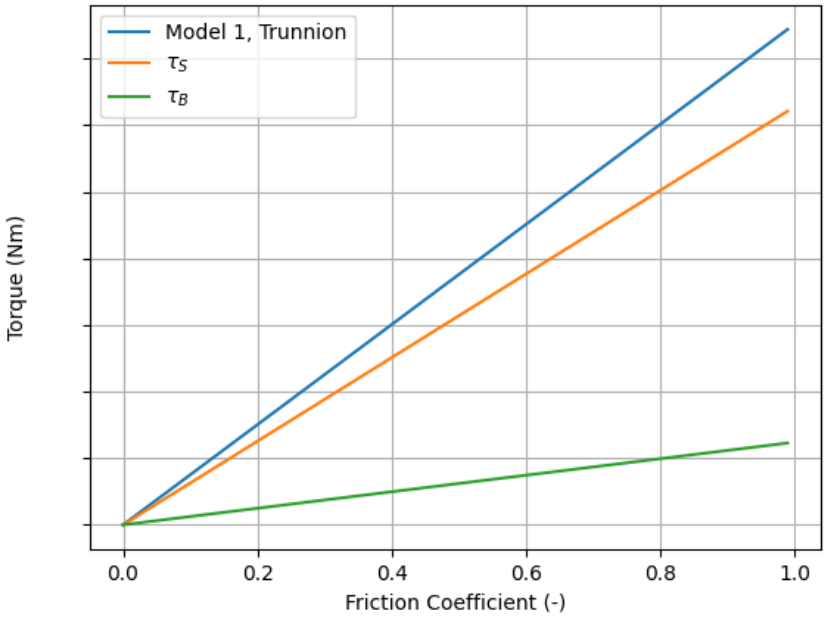

Figure 4.3: Sensitivity study of torque estimation model 1. Both torque components (T_S & T_B) are plotted as functions of the friction coefficient (orange and green lines respectively), as well as their summation (blue line).

As expected, the relation of both torque components to the friction coefficient is completely linear. This means that choosing the friction coefficient value when estimating torque values is crucial, and results obtained from this simple estimation method should also consider differing friction coefficient values.

4.2.2. Torque Estimation Model 2 Analysis

Unlike model 1, the second torque estimation model depends on 5 separate components. Out of these 5 components, 4 depend on friction coefficient. The hydrodynamic torque component (T_H) is independent of any friction coefficient. As such, T_H will not be considered in this sensitivity analysis.

Recalling Equation (4.3), Equation (4.4) and Equation (4.19), the first two are directly proportional to a friction coefficient. The third equation is also directly proportional to a friction coefficient (as shown in Equation (4.17)). Because of this, it is expected that the relation between torque values and friction coefficients will be similar to the one seen in Section 4.2.1.

Figure 4.4 shows the sensitivity analysis for model 2. As expected, a variation in friction coefficient

results in a linear increase of all torque components (except for the excluded hydrodynamic torque).

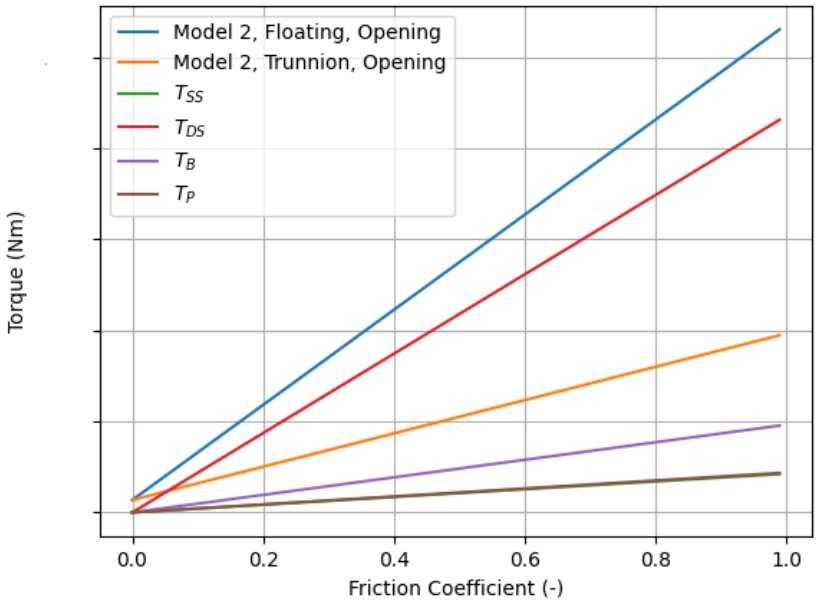

Figure 4.4: Sensitivity study of torque estimation model 2. All torque components (T_SS, T_{DS}, T_B & T_P) are plotted as functions of the friction coefficient (green, red, purple and brown lines respectively), as well as their summation (blue line for floating ball valve, orange line for trunnion).

As seen in the figure above, the packing and the bearing torque components are the least sensitive to friction coefficient variations, while the largest component of the overall torque is the dynamic seat torque, T_{DS}.

From Figure 4.4, similar conclusions as in Section 4.2.1 can be drawn. This model, just like model 1, heavily depends on the friction coefficients chosen. Because of this phenomenon, it is recommended to consider multiple friction coefficient values when evaluating the torque required for a specific ball valve.

4.3. Torque Models Validation

During several testing campaigns, it was possible to obtain torque data for a valve prototype of known dimensions. This data was subsequently stored, and was made available internally. This limited amount of data allows validation of the torque models presented in Section 4.1. The purpose of this section is to concisely present the validation of both torque models, using experimental torque data.

The first step in the validation process was to gather experimental data by which the torque values obtained from model 1 and model 2 could be compared. The Propulsion Testing team at PLD Space provided this experimental raw data, along with the properties and dimensions of the valves used. Two different types of valves were used in these tests - a floating ball valve and a trunnion ball valve, with their general features discussed in Section 2.3.4.

The data gathered was torque data required to open these two types of valves, at a certain temperature and pressure. Both valves were tested in cryogenic conditions, at varying pressures from 50 bar all the way up to 108 bar. Average torque values were taken for each experiment, and were subsequently compared to torque values obtained by using model 1 and model 2. Although the torque values can not be revealed, the error of each model (at a specific pressure) was calculated, and can be found in Table 4.1.

Table 4.1: Error of both models used to estimate torque values, compared to experimental data[1].

	Floating Configuration				Trunnion Configuration			
Pressure (bar)	50	70	90	108	50	70	90	108
Model 1 Error (%)	-	-	-	-	-	-	1.211	-4.888
Model 2 Error (%)	-0.359	-8.409	-0.005	-5.844	-	-	11.681	9.002

According to the table presented above, model 1 has an error of less than 5%. This is despite of how simple of an estimation method model 1 is - as it only depends on 2 equations, and a total of 4 variables.

In contrast to model 1, torque estimation model 2 shows a higher degree of error in its values. For the floating ball valve, the error does not surpass 8.5%, while for the trunnion ball valve the error goes up to 11.7%. This model seems to be more accurate when it comes to estimating torque values for floating ball valves.

In the application of this model to the ball valve under consideration, it must be noted that said valve will be working under cryogenic conditions (as per **BV.2**). These conditions may affect the surface properties of the seat materials, which in turn could result in a change in the friction coefficient between the valve seats and the ball, which could greatly vary the torque needed to operate the valve. This effect must be taken into account during torque estimation, although the extent of this effect heavily depends on the material chosen for the valve seats.

4.4. Conclusions

Throughout this chapter, two torque estimation models have been presented. Model 1, taken from the Aerospace Fluid Component Designer's Handbook [21], consists of 2 simple equations which depend on pressure, port diameter, and two friction coefficients. This model is able to estimate the maximum torque required to operate a trunnion ball valve.

Model 2, found in 'Air-Operated Valve Evaluation Guide' [20] and combined with the static seat torque model from 'The Optimisation of the Floating Ball Valve Seat Component Design Methodology' [18], depends on a total of 5 equations, which have as input a multitude of variables. This torque estimation method is significantly more complex than model 1, but as a result it can estimate the maximum required torque for both floating and trunnion ball valves, during either opening or closing of the valve.

Both models were explained in length during Section 4.1.1 and Section 4.1.2, and were implemented into a Python script (which can be found in Appendix A). Following their implementation, a snesitivity analysis was carried out on all of the components of both torque estimation models - documented in Section 4.2. During this analysis it was found that most torque components are directly proportional to the friction coefficients chosen for each component (μ_S, μ_B and μ_P). This highlights the criticality of choosing friction coefficients when estimating the torque required to open a ball valve.

In order to verify the validity of both of the models presented, it was decided to validate these models via comparison of torque values with experimentally-obtained torque values. Data of the valves used in experiments was readily available, as well as torque data for each experiment. Experimental data was processed, and compared to estimations from both torque models presented. The findings are shown in Section 4.3. It was found that model 1 was quite accurate in estimating trunnion ball valve torque (with errors of less than 5%). Model 2 was found to be moderately accurate when estimating torque values for floating ball valves (errors of less than 8.5%), however its accuracy was significantly reduced when estimating trunnion ball valve torque values (with errors from 9 up to 11.7%).

[1] Note: Torque estimation model 1 is only valid for trunnion ball valves, hence only trunnion torque data was considered in the validation procedure of this model.

5

Flow Factor Model

The flow factor K_v (also known as the flow coefficient (C_v), in the imperial system) is a value by which the 'efficiency' of a component at passing fluid through itself can be quantified. Its units are m3 / h, hence this variable indicates how much volume of a certain fluid passes through a component per hour.

In the design of a ball valve, the minimum flow factor is usually a requirement on the component. This component requirement is set by the engine system requirements, specifically that of the required propellant flow into the combustion chamber. Having a minimum flow factor value results in the guarantee of a specific fluid flow rate through the valve.

Although requirements do set a minimum required K_v (flow factor) as stated in requirement **BV.8**, this value refers to the minimum K_v when the valve is fully open - that is, the position at which the port within the ball is fully aligned with the direction of the fluid flow. In this position, the ball valve has its maximum K_v, whereby its internal profile resembles that of a pipe - its K_v will be equal to that of a pipe with the length of the ball valve.

Due to the process by which a ball valve is opened (rotating the ball from 0º to 90º as to allow flow through) it is useful to know the K_v value of the valve as the ball rotates. Knowing the K_v value as a function of the valve opening helps in the analysis of the start-up procedure of the engine. The purpose of this chapter is to show the methodology by which this value was estimated.

The chapter is structured as follows. Section 5.1 documents the implementation of a set of equations to calculate the geometrical opening area of a ball valve as a function of opening angle. Section 5.2 is a brief verification of the geometrical area model. Section 5.3 presents the methodology by which the flow factor of the ball valve as it opens is calculated, as well as results of said methodology. Finally, Section 5.4 which gives an overview of the entire chapter and discusses findings.

5.1. Geometric Area Model

The first step in the process of calculating the flow factor of the ball valve is calculating the geometric opening area of the valve - which refers to the area available for the fluid to flow through the valve - as a function of the ball's rotation angle. The relevance of this term in the K_v calculations can be seen if the flow factor equation is analysed. The flow factor equation is shown in Equation (5.1).

$$K_v = Q \cdot \sqrt{\frac{SG}{\Delta P}} \tag{5.1}$$

As seen above, the flow factor equation depends on 3 terms: Q, which is the flow rate (in m^3/h), SG, which is the specific gravity of the fluid, and Δ P, which is the pressure loss (in this case across the

valve) in bar. The relevant term here is the flow rate Q. The equation for flow rate is given below.

$$Q = \dot{m} \cdot \frac{3600}{\rho} \tag{5.2}$$

Where $\dot{m}$ is the mass flow of fluid through the valve (in kg/s) and ρ is the density of the fluid (in kg/m^3). Using the equation for mass flow ($\dot{m} = \rho A v$), Equation (5.2) can be rewritten into the following.

$$Q = A \cdot v \cdot 3600 \tag{5.3}$$

Where A is the area of flow (in m^2) and v is the flow velocity (in m/s), which is assumed constant as the ball valve is opened. Plugging this back into Equation (5.1) results in the following expression.

$$K_v = 3600 \cdot A \cdot v \cdot \sqrt{\frac{SG}{\Delta P}} \tag{5.4}$$

With Equation (5.4), it can be seen that K_v is directly proportional to the area of flow - hence making it a critical variable that must be known in order to calculate K_v.

In order to calculate the geometric opening area, it is assumed that the area to be calculated is that of an intersection between two circles (the ball's bore, and the valve's bore). This is illustrated in the figure below.

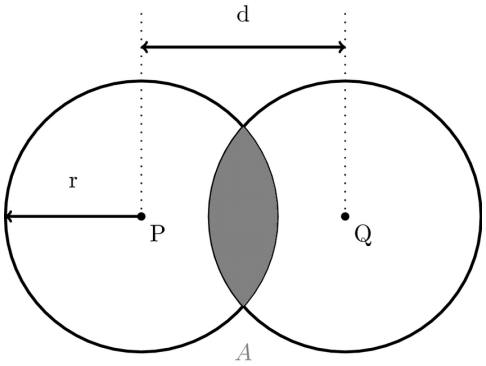

Figure 5.1: Area of intersection A between two circles with the same radius r, whose centers P and Q have distance d from each other [37].

In this specific case, it is assumed that both circles have the same radius (that being the radius of the bore). The area shown in grey in Figure 5.1 is given by the following equation [16].

$$A = r_1^2 \cdot \left(\frac{\alpha_1 \cdot \pi}{180} - \cos\left(\frac{\alpha_1 \cdot \pi}{180}\right) \cdot \sin\left(\frac{\alpha_1 \cdot \pi}{180}\right)\right) + r_2^2 \cdot \left(\frac{\alpha_2 \cdot \pi}{180} - \cos\left(\frac{\alpha_2 \cdot \pi}{180}\right) \cdot \sin\left(\frac{\alpha_2 \cdot \pi}{180}\right)\right) \tag{5.5}$$

Where r_1 is the radius of the first circle, r_2 is the radius of the second circle, α_1 is the angle between the line PQ and the intersection of the circles for the first circle, and α_2 is the same angle but for the second circle.

In this case, since it has been established that both circles have the same radius (r_1 = r_2 = r), the angles α_1 and α_2 will be equivalent (α_1 = α_2 = α). Rewritting Equation (5.5):

$$A = r^2 \cdot \left(2 \cdot \frac{\alpha \cdot \pi}{180} - 2 \cdot \cos\left(\frac{\alpha \cdot \pi}{180}\right) \cdot \sin\left(\frac{\alpha \cdot \pi}{180}\right)\right) = r^2 \cdot \left(\frac{\theta \cdot \pi}{180} - \sin\left(\frac{\theta \cdot \pi}{180}\right)\right) \tag{5.6}$$

Where θ = 2·α. In order to calculate the value of θ, Equation (5.7) is used.

$$\theta = 2 \cdot \arccos\left(\frac{r - \frac{x}{2}}{r}\right) \cdot \frac{180}{\pi} \tag{5.7}$$

Where r refers to the bore radius, and x refers to an array that goes from 0 up to a value of twice the radius (representing the gradual opening of the valve). This relation is derived from geometry. With this, a function can be drafted in a Python script, that can calculate the area of flow from right when the valve is about to open (when the circles are barely touching) up to when the circles are completely overlapped (and the ball valve is fully opened).

In order to relate the value of the opening area A (given by Equation (5.6)) and the opening angle of the valve, an equation is drafted using the aforementioned variable 'x'. This variable serves as a way to measure the degree to which the valve is open, as a distance. The following equation has been produced from geometry, and transforms x into opening angle.

$$\gamma = \arccos\left(1 - \frac{x^2}{2r^2}\right) \cdot \frac{180}{\pi} + \left(\arccos\left(\frac{r}{r_{out}}\right) - \arcsin\left(\frac{r}{r_{out}}\right)\right) \cdot \frac{180}{\pi} \tag{5.8}$$

Where γ is the opening angle in degrees (closed at 0º, and fully open at 90º), and r_{out} the radius of the ball. The second term is added to the first term (which depends on x) to account for the offset in opening angle. This second term only depends on the inner bore radius and the outer ball radius, r & r_{out} (the ratio between bore size and ball size). This 'offset' refers to the fact that for up to a certain angle (which depends on the aforementioned ratio) the area of flow through the valve will remain at 0, as the ball's bore and the valve's bore do not intersect. The second term in this equation calculates the ball's rotation angle at which these two 'circles' (the ball's bore and the valve's bore) are barely intersecting.

The methodology and equations presented above were implemented into several functions within a Python script. Using geometric data from different valves, the following figure was produced using said script.

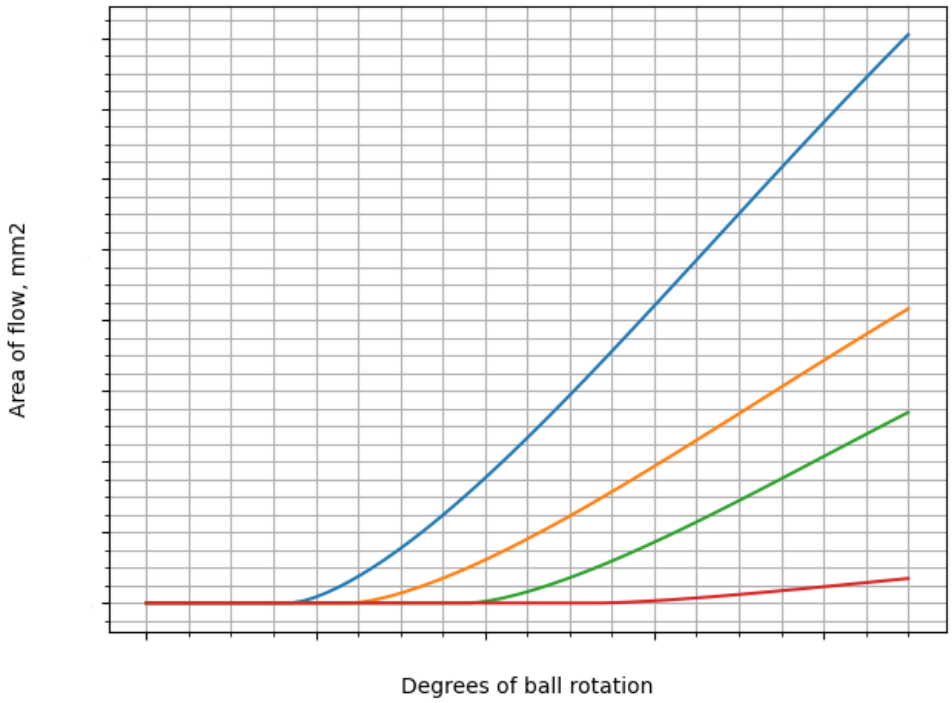

Figure 5.2: Area of flow vs. ball rotation for 4 different ball valves, of decreasing bore size. The blue line represents the biggest valve, and the red line represents the valve with the smallest bore.

Only two geometrical measurements are used as input in the area calculation function - the valve's bore diameter and the ball's bore diameter.

5.2. Geometric Area Model Verification

After the opening area calculation function was completed, it was implemented in a Python script, which is shown in Appendix B. The implementation of the calculations into the code was verified using different methods. The purpose of this section is to document the methods used to verify the results obtained using the opening area calculation function.

5.2.1. Hand Calculations

The first - and simplest - method used to verify the Python code was hand calculations. Although the area distribution as the valve is opened is not trivial, it can be assumed that:

- At 0º, the ball's bore is perpendicular to the valve's bore - therefore the area of flow will be 0.
- At 90º, the ball's bore directly coincides with the valve's bore - therefore the area of flow will be at a maximum.

As seen in Figure 5.2, at the origin of the graph (all the way to the left of the graph) every single line plotted has an area of flow of 0. As stated above, this is to be expected due to the position of the ball when its rotation is 0º.

Verifying the second assumption is not as trivial. When fully opened, the area of flow is equal to that of the area of a circle ($\pi \cdot r^2$). Recalling Equation (5.6) and Equation (5.7), when the valve is fully open the value of x becomes $2 \cdot r$. Plugging this value back into Equation (5.7) results in a value of θ of 180º. If this value of θ is then plugged into Equation (5.6), one can simplify this equation as follows.

$$A = r^2 \cdot \left(\frac{\theta \cdot \pi}{180} - \sin\left(\frac{\theta \cdot \pi}{180} \right) \right) = r^2 \cdot \left(\frac{180 \cdot \pi}{180} - \sin\left(\frac{180 \cdot \pi}{180} \right) \right) = r^2 \cdot (\pi - \sin(\pi)) = \pi \cdot r^2 \quad (5.9)$$

As shown above, when the valve is fully opened, the area obtained using the area opening function is the same as that of a circle. This can be manually verified by calculating the area of a circle with a certain radius, and then plugging in this same radius into the Python script, and checking the figures generated. At the 90º opening angle, the area will be equal to the manually-calculated area of a circle, as demonstrated above.

5.2.2. CAD Verification

The second method by which the geometrical opening area results were verified was by using a CAD model. The CAD model used was of a specific, readily-available ball valve.

Through CAD software, the ball within the ball valve was gradually rotated from its closed position at 0º up to its fully open position at 90º, in 5º intervals. At each position, the opening area was measured using CAD software tools, and noted in an Excel sheet - later imported into the Python script.

This procedure was then followed by taking measurements of the geometry of the CAD model, and inputting these into the opening area calculation function described in the previous section. Both the calculated area and the CAD-measured area were subsequently plotted in Figure 5.3 for comparison.

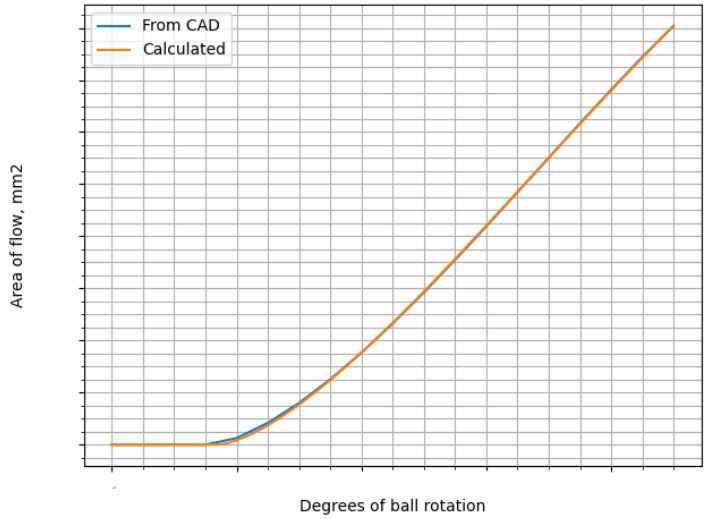

Figure 5.3: Area of flow vs. degrees of ball rotation calculated using CAD software (blue line) and using the geometric area model (orange line). Both lines overlap for most of the ball's rotation, except in the very early opening angles where it seems like the model slightly underestimates the opening area.

Apart from minor incongruities in the lower ball rotation area, it can be seen that the calculated area closely follows the measured CAD area.

5.2.3. Comparison With Prior Data

The final method by which the opening area function was verified was by using two readily-available valves, of which there is data of area of flow vs. degrees of ball rotation available.

The data for these two valves was available only as a graph of flow passage area vs. opening stroke (in percentage), so to compare the results obtained with the opening area function, an identical plot was generated. In order to generate this plot, physical measurements were taken of the geometry of both of these ball valves, and the values obtained were then used as input for the opening area function as presented in Section 5.1.

The result of this procedure was another graph, identical to the already available flow passage area vs. opening stroke plot for the 2 ball valves. To check this, the generated plot was overlaid on the original graph. The results of this are shown below.

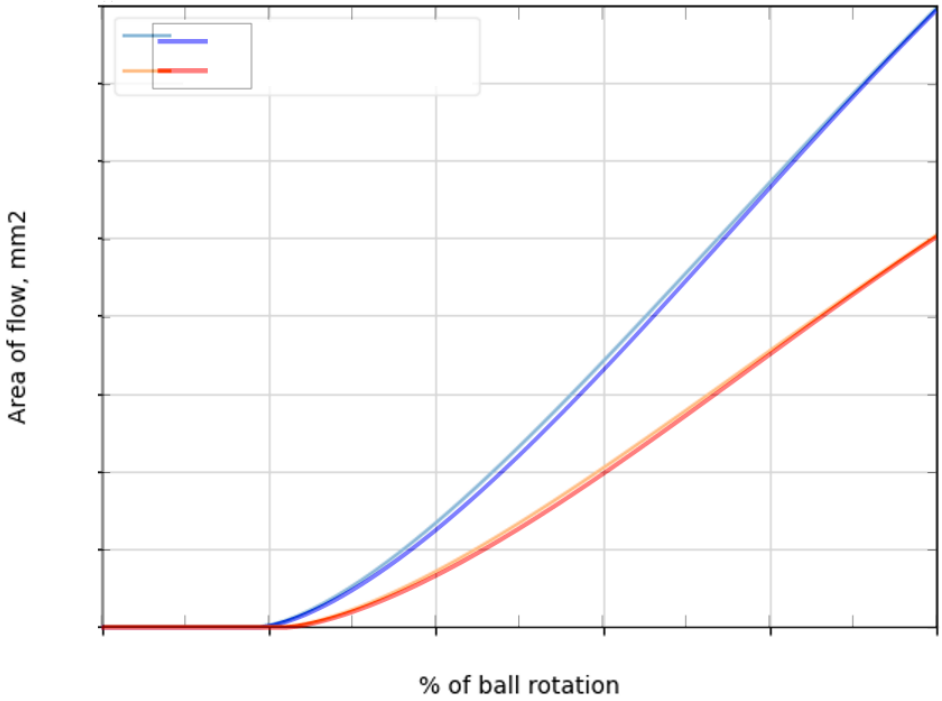

Figure 5.4: Comparison of calculated area of flow using the methodology explained above, versus area of flow data obtained from commercial ball valves, with known geometry. This is shown for two different valves, where the light & dark blue lines represent valve 1, and the orange & red lines represent valve 2 (of considerably smaller size).

Despite the rudimentary method used, Figure 5.4 shows that the calculated opening area coincides with the flow passage area from available historical data for both valves (the blue and orange lines).

5.3. Flow Factor Calculation

Having drafted a function which can calculate the flow passage area as a function of the opening angle of a ball valve, the flow factor can be calculated next. The purpose of this section is to present the methodology followed to calculate the flow factor as a function of the ball valve's opening angle.

Looking back at Equation (5.4), and taking into account the assumption that the term 'v' remains constant, only two other variables are needed in order to calculate the value of the flow factor. These are the specific gravity (SG) of the fluid flowing through the valve, and the pressure drop across the valve (ΔP).

The former value is a constant and only depends on the fluid. For liquid oxygen (LOX), this value is 1.14 [36]. Valves working with a different fluid will have different SG values. The latter (ΔP) is a variable which depends on the geometry of the component. In the case of a ball valve, the pressure drop will not be a constant value due to its geometry change as the ball valve is opened.

In the estimation process of ΔP, a CFD simulation could hypothetically be set up in which the pressure drop across the ball valve is calculated with the ball at different positions - starting from a fully closed valve at 0º, and increasing this angle by small increments up until the valve is fully open (at 90º). This is a potential solution to finding the value of ΔP as the angular position of the ball changes. However, it was decided to not go with this approach as the scope of this research project did not concern itself with CFD analysis.

The alternate approach chosen was to use experimental data in order to estimate the value of ΔP as the opening angle changes. In order to obtain the experimental data to do this, the Testing team drafted and executed a test campaign whereby an analogous ball valve (to the one considered in this research project) was tested in certain operational conditions (the same as the valve being considered).

The valve was first closed, with its upstream side pressurized, and the ball was rotated via a motor up to certain opening percentages. The pressures upstream and downstream were recorded, and this data was analysed as to calculate the pressure drop across the valve with different opening angles.

With said pressure drop data available, a rough empirical relation was produced. This relation is shown below, in Equation (5.10).

$$\Delta P = 3.770044 \cdot e^{-0.026731 \cdot \gamma} \tag{5.10}$$

Where γ refers to the opening angle of the ball valve, in degrees. It must be noted that this pressure drop relation is unique to this specific ball valve - other ball valves with different bore sizes and different ball designs may have a different pressure drop distribution.

Referring back to Equation (5.4), all three variables are now known. Using the procedure presented in Section 5.1 and other equations presented in this chapter, a Python script was produced. This script takes as input geometric data from a ball valve, as well as its operating conditions, and in return can generate an approximation of the K_v value as the ball valve is opened. This script (along with all of the relevant functions) can be found in Appendix B.

Using said script, figures such as Figure 5.5 can be generated.

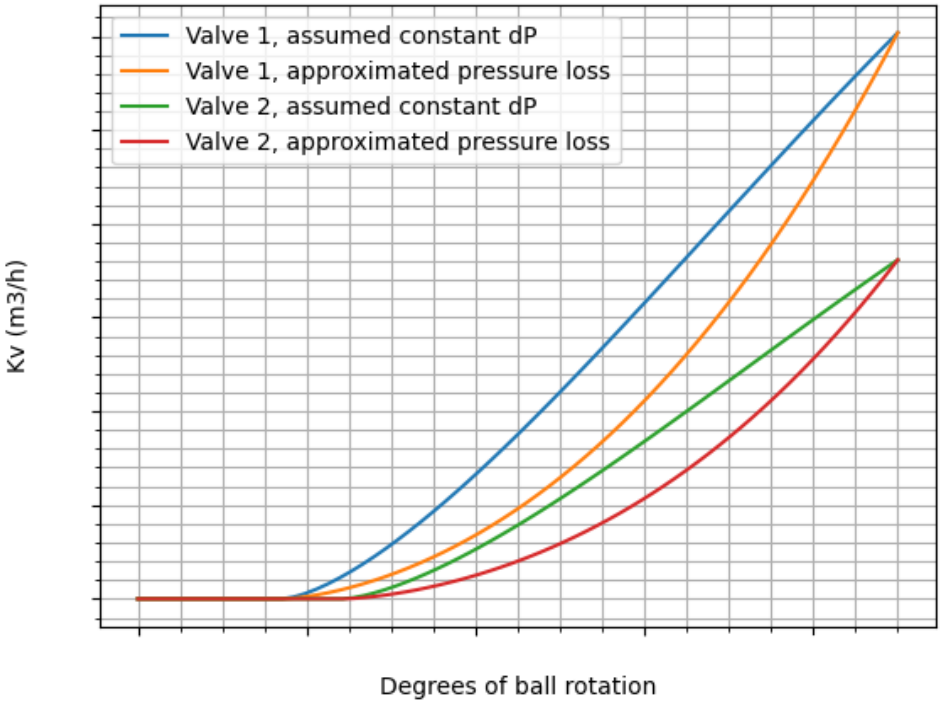

Figure 5.5: Flow factor (K_v) plotted against degrees of ball rotation for two different ball valves, 'Valve 1' and 'Valve 2'. Two lines are shown per valve - one using a constant pressure loss, and one using an approximated pressure loss distribution as the valve is opened.

This figure contains the K_v curves for two different valves. The first two curves are for "valve 1", representing the variation of K_v as the valve is opened. The first curve (in blue) was drafted through the assumption that the pressure loss across the valve (ΔP) is constant (and equal to the pressure loss when the valve is fully opened). The second curve considers the ΔP distribution presented in Equation (5.10). By comparing these two curves, the difference in constant and variable pressure loss across the valve can be observed.

The second pair of curves are similar to the first two, but instead consider a different, smaller valve. As a result, valve 2 can achieve a smaller K_v overall.

With the possibility of being able to determine K_v as a function of the valve's ball rotation, it can now be determined the rotation point at which a ball valve is delivering more than the required K_v, according to requirement **BV.8**.

5.4. Conclusions

The purpose of this chapter was to show a methodology by which the flow factor of a ball valve can be estimated, as a function of the valve's opening angle.

In order to estimate the flow factor of a ball valve as it opens, the geometric opening area of the valve must be known. This area refers to the area available for the fluid to flow through the valve. A method to calculate this value (as a function of the opening angle of the ball of the valve) is presented in Section 5.1. The methodology presented assumes that the geometric opening area is equal to the intersection area of the two ports (the ball's bore and the valve port) which are assumed to be of equal size (full bore valve).

In order to prove this methodology as coherent, it was decided to verify the geometric area calculation process. To do this, three different verification approaches were taken, which are all listed below.

- Hand calculations - making sure that at 0º turning angle the intersection area is equal to 0, and that at 90º turning angle the intersection area is equal to the area of a full circle.
- CAD verification - comparing the area values obtained using the methodology presented with values measured from a CAD model of a valve with known geometry.
- Comparison with prior data - area of flow vs. % of ball rotation figures were available for two separate valves, where their geometries were known, hence allowing comparison with the area values obtained with the methodology presented.

With these three methods, the geometric area model was verified successfully.

Having a model by which the opening area of a ball valve can be calculated as a function of the opening angle, the next step was to calculate the flow factor, K_v. This factor mainly depends on the fluid flow rate through the valve (which directly depends on the opening area) but it also depends on the pressure loss across the valve. This value is straightforward to estimate when a ball valve is fully open (acting as a straight pipe) but calculating pressure loss in a partially-open ball valve is a more complicated matter. For this reason, it was decided to make use of readily-available experimental data a ball valve test, where the upstream and downstream pressures were measured. This data was used to approximate a pressure loss distribution as the ball valve is opened. With this estimation, the flow factor was calculated (as presented in Section 5.3).

The results of this chapter are as follows. First, a method by which the opening area of a ball valve can be calculated only using geometrical data of the valve as input. Secondly, a method to estimate the flow factor across a ball valve as the valve is opened. Both of these functions were implemented into a Python script, which is presented in Appendix B. With this script (and the figures generated therein) the ball rotation angle at which the minimum required flow factor (as specified in requirement **BV.8**) is achieved can be found. This may be useful in the modelling of the start-up procedure of an engine which makes use of ball valves for its primary feed lines.

6

Valve Weight Optimization

Due to the strict mass budgets imposed on rocket engines - with the intent of maximizing the payload mass delivered to orbit - it is of interest, when designing a rocket engine, to keep the mass of its individual components to a minimum. Ball valves are systems commonly found in rocket engines, and as a result it is of interest to develop a procedure by which the weight of these systems can be minimized.

The purpose of this chapter is to document the methodology followed in order to optimize the design of a ball valve, in order to have a ball valve design which complies with the requirements listed in Section 2.1.

The structure of this chapter is as follows. The first section, Section 6.1, lists the assumptions for the entirety of this chapter. Section 6.2 documents the equations which drive the thickness optimization process, and introduces the main stress component. Section 6.3 presents the Ashby material selection procedure in order to both select a set of appropriate materials and finish the weight optimization. Section 6.4 presents the results from the Ashby material selection procedure, including optimized thicknesses for the chosen material alloys, approximated weights for each, and their (also approximated) price of manufacture. This section is followed by Section 6.5, which briefly documents the verification procedure for the weight optimization process and the corresponding results. Finally, Section 6.6, which concludes the chapter and compiles its findings.

6.1. Assumptions

Ball valves are complex systems composed of a plethora of components, many of which can be optimized for weight. In order to simplify the problem at hand, it was decided to undertake a certain number of assumptions.

- The ball valve is assumed to be an infinitely-long tube.
- It is assumed that said tube has thick walls.
- It is assumed that the outer (atmospheric) pressure (P_{out}) is lower than the inner (valve) pressure (P_{in}).

Since the ball valve is assumed to be a tube, the inner diameter of said tube is equal to the inner diameter of the ball valve (which is a fixed value, dependent on several flow factors).

The 'thick walls' assumptions implies that $\frac{t}{d_i} > \frac{1}{20}$, where t is the thickness of the tube, and d_i is the inner diameter of the tube.

6.2. Thickness Optimization

With the previously-presented assumptions in mind, the minimum thickness required for the assumed vessel can be calculated. This section documents the process by which the minimum thickness of an infinitely-long cylindrical vessel can be calculated.

The stresses experienced by the assumed vessel are given by the following equations [45].

$$\sigma_{axial} = \frac{P_{in} \cdot R_{in}^2 - P_{out} \cdot R_{out}^2}{R_{out}^2 - R_{in}^2} \tag{6.1}$$

$$\sigma_{hoop} = \frac{P_{in} \cdot R_{in}^2 - P_{out} \cdot R_{out}^2}{R_{out}^2 - R_{in}^2} - \frac{R_{in}^2 \cdot R_{out}^2 \cdot (P_{out} - P_{in})}{R^2 \cdot (R_{out}^2 - R_{in}^2)} \tag{6.2}$$

$$\sigma_{radial} = \frac{P_{in} \cdot R_{in}^2 - P_{out} \cdot R_{out}^2}{R_{out}^2 - R_{in}^2} + \frac{R_{in}^2 \cdot R_{out}^2 \cdot (P_{out} - P_{in})}{R^2 \cdot (R_{out}^2 - R_{in}^2)} \tag{6.3}$$

Where σ_{axial}, σ_{hoop} and σ_{radial} refer to the axial, circumferential and radial stresses experienced by the vessel, P_{in} is the inner vessel pressure (so the pressure of the valve), P_{out} is the outer (atmospheric) pressure, R_{in} is the inner radius of the vessel, R_{out} the outer radius of the vessel, and R the radial position at which the stress is being calculated. For this exercise, it is assumed that the maximum stress will happen when R = R_{in}. Due to the high working pressures of the valve (P_{in} » P_{out}) it is assumed that P_{out} = 0, which greatly simplifies the aforementioned equations.

Geometry dictates that the thickness of the vessel (t) is given by:

$$t = R_{out} - R_{in} \tag{6.4}$$

This equation can then be plugged into Equation (6.1), Equation (6.2) and Equation (6.3) to obtain 3 separate expressions, each relating thickness to their respective stress type. With a chosen R_{in} (from geometry) and a P_{in} (from requirements) the relationship between thickness and different types of stress can be plotted. An example of this is given in Figure 6.1.

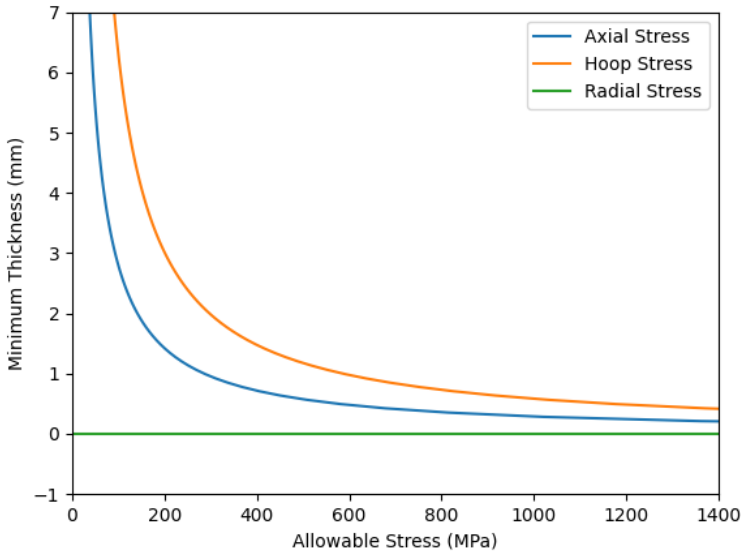

Figure 6.1: Minimum vessel thickness vs. allowable stress, for an infinitely-long thick-walled cylinder, where P_{out} is assumed to be 0.

During the manual work-out of Equation (6.1), Equation (6.2) and Equation (6.3), it was observed that most terms cancelled out in Equation (6.3), making radial stress insensitive to thickness. For this reason, it is shown as a flat, green line in Figure 6.1.

As Figure 6.1 shows, the hoop (circumferential) stress is the limiting stress, meaning that this stress requires the highest vessel thickness. This is due to the high pressure difference between P_{in} and P_{out},

which makes σ_{hoop} the most significant stress component out of the three considered stress types.

Having the capability to generate figures such as the one shown in Figure 6.1 means that one may determine the minimum required thickness of the cylindrical vessel if the maximum allowable stress of the material used is known.

6.3. Ashby Material Selection

With the information presented in Section 6.2, the mass optimization of the valve (through the usage of Ashby material selection) can proceed.

The Ashby material selection procedure allows for material selection using a performance parameter and Asbhy plots. The performance parameter depends on the problem being considered. The derivation of the performance parameter for the valve mass optimization problem is shown below.

The mass of our simplified valve (a cylinder) is given by the following equation.

$$m = \rho \cdot V = \rho \cdot \pi \cdot L \cdot (R_{out}^2 - R_{in}^2) \tag{6.5}$$

Where ρ refers to the density of the material used, V is the volume, and L is the length of the cylinder (assumed finite length so that its mass can be calculated). Since P_{in} is significantly larger than P_{out}, σ_{hoop} is most significant stress factor (as shown in Section 6.2). With this in mind, Equation (6.2) can be rearranged as follows:

$$(R_{out}^2 - R_{in}^2) = \frac{1}{\sigma_{hoop}} \cdot k \tag{6.6}$$

where

$$k = (P_{in} \cdot R_{in}^2 - P_{out} \cdot R_{out}^2) - \frac{R_{in}^2 \cdot R_{out}^2 \cdot (P_{out} - P_{in})}{R^2} \tag{6.7}$$

With this rearrangement in place, Equation (6.6) can be substituted into Equation (6.5), resulting in the equation shown below.

$$m = \frac{\rho}{\sigma_{hoop}} \cdot \pi \cdot L \cdot k \tag{6.8}$$

Since the goal of this exercise is to minimize the mass (m), assuming the other parameters remain constant (L, k) mass could be minimized by minimizing the value of $\frac{\rho}{\sigma_{hoop}}$, or inversely maximizing the value of $\frac{\sigma_{hoop}}{\rho}$. The last term presented is commonly referred to as the 'performance parameter'.

This performance parameter can then be plotted as a straight line on an Ashby plot, such as the one shown below.

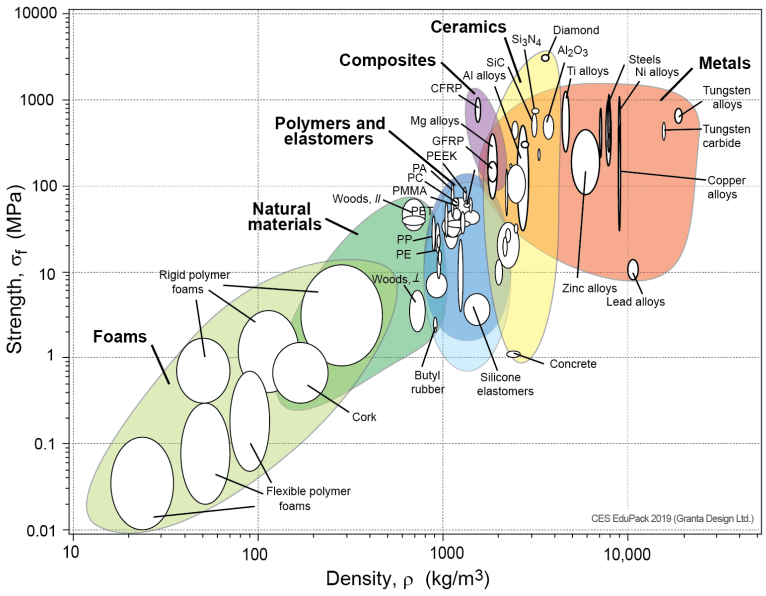

Figure 6.2: Strength σ_f vs Density ρ materials chart [14].

By plotting the performance parameter on said plot, one can compare performances of different material types, and rule out certain materials. Once the satisfactory materials have been selected, the material properties can be used as input for the equations previously presented, so that data such as the minimum thickness or the approximate mass of the valve body can be found.

6.4. Results

The purpose of this section is to present the results of the previously-explained material selection procedure, by showing a list of possible material candidates, and comparing each one using attributes such as the mass or the cost of the final valve body. By the end of this section, a recommendation on the material to be used in the final valve design will be given, along with an optimal valve body thickness.

The first step to obtain results is to limit the number of materials that will be considered for the valve body. This has already been described in the section prior. Using Figure 6.2, the performance parameter previously found ($\frac{\sigma_{hoop}}{\rho}$) can be plotted as a straight line. This is shown in Figure 6.3, where the performance parameter is plotted as the red lines.

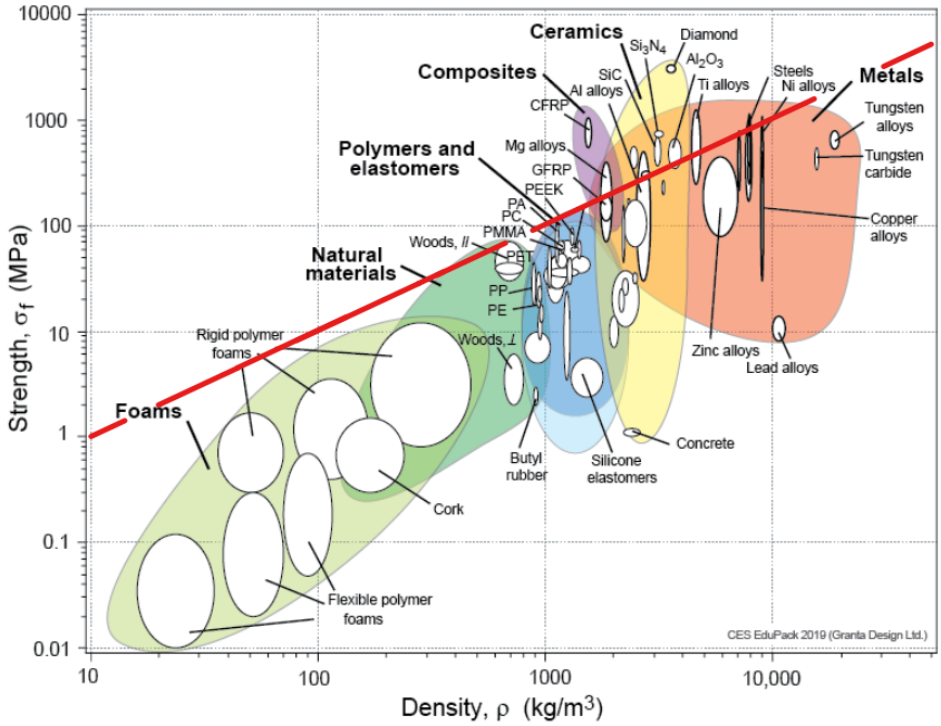

Figure 6.3: Strength σ_f vs Density ρ materials chart [14], including a red line which represents the performance parameter for the weight optimization of a cylinder, $\frac{\sigma_{hoop}}{\rho}$.

The red lines shown can be moved as to limit the number of materials being considered. Every material that lies on the red line has the same performance (with respect to the performance parameter found). As shown in the figure, the line was shifted upwards, as to select the four following alloys:

- Nickel alloys
- Aluminium alloys
- Steels
- Titanium alloys

According to the Ashby plot, these four alloys should have roughly similar performance parameter values. With these alloys selected, one can go to a materials library and select the highest-performing (strength-wise) alloys from each category, and calculate the required thickness for each material. This can be done using the yield strength of each selected material, and plugging it into Equation (6.2). R_{in} is fixed[1], P_{in} is also fixed, and P_{out} can be assumed to be 0 (as P_{in} » P_{out}). With this, the thickness can be found. Alternatively, one may use the figures generated from these equations, such as the one shown in Figure 6.1.

Once thickness for each material has been obtained, other values (such as mass) can be calculated. This will help in choosing the final material to be used for the valve's body. This is shown in Table D.2. This table also includes rough estimates of the prices of each selected material, which is meant to help with the final material selection.

From the table, it can be seen that the top performing materials (mass-wise) are the titanium, aluminium and nickel alloys. In terms of cost, aluminium is the cheapest, while the nickel alloy is the heaviest. Taking into account both of these metrics, it seems that the titanium alloy is the most sensible candidate for the material of the valve body. This is due to its extremely low mass, and its reasonable

[1]The value of R_{in} is set to the largest inner radius in the valve - in this case, the valve body cavity, where the ball is housed. This is because taking the largest radius results in the worst case scenario (higher stresses).

price.

This conclusion would be valid for a non-cryogenic ball valve, where the effects of extremely low temperatures do not have to be taken into account. Due to the case being considered in this research, the material selection is affected by this constraint. Both titanium and aluminium alloys have been shown to have a tendency of self-ignition when exposed to fluid flow at cryogenic temperatures [35]. This is in direct violation of valve requirement **BV.13**, disqualifying both materials for use in cryogenic conditions due to this risk, and consequently disqualifying them for the valve body material as well.

This means that, based off the results from Table D.2, the nickel alloy valve body is the optimal material. This is a great option due to the significantly low mass of the valve body, while keeping the cost moderately low. Steel remains as the back-up option, with the downside of an increased mass. Titanium and aluminium still remain superior choices, but are definitely not to be considered in cryogenic ball valves.

6.5. Weight Optimization Verification

The purpose of this section is to briefly present the verification method taken to corroborate the findings presented in Table D.2 in Section 6.4.

The thickness of each valve body - depending on their material - assigned in the previous section directly depends on the yield strength of said material, and the assumed inner pressure within the valve body (which is a constant for all valve bodies). In order to verify these assigned thicknesses, one must subject the different valve bodies to the target (inner) pressure, and probe the stresses experienced by the valve bodies while under pressure - assuming the valve is closed.

To inquire into the stresses experienced by the valve body, a static structural analysis case was set up for each valve body (one per material chosen). This was implemented in the analysis software ANSYS, and the details of the set-up procedure and detailed results are shown in Section 7.2 and Section 7.3 respectively, from Chapter 7. These analysis cases take into account pressure forces, and also the cryogenic temperature the valve bodies will experience when in operation.

From the results obtained during the analysis process the points of each valve body at which stress peaked was noted, and the stress value at this point was recorded. The findings of this analysis and the comparison to the yield strength of each material can be found in Table 6.1 below.

Table 6.1: Comparison of yield strength of the valve body materials, versus the peak stress each valve body experienced in analysis.

	Maximum Stress (Mpa)		**Error (%)**
	Yield Strength	**Analysis Data**	
Aluminium	405	419	3.457
Steel	220	245	11.364
Nickel	1034	989	-4.352
Titanium	813	832	2.337

In the table, it can be seen that the stresses measured in the static structural analysis cases are slightly higher than the yield strength of the chosen materials (up to 11.4% higher than expected). This is applicable for all the materials except the nickel alloy. In order to ensure the stresses experienced in the valve body do not go over the yield strength of each material, it is recommended to apply a safety margin of 20%, as to ensure the structural integrity of the ball valve[2].

[2] It is worthy to note that the inner pressure that the 4 valve bodies were subjected to during analysis is 1.5 times the maximum pressure the valve will experience during its expected operating conditions. Hence the results discussed in this chapter are considered to be conservative.

6.6. Conclusions

Throughout this chapter, a methodology of valve weight optimization has been presented.

In order to begin the weight optimization procedure, first a set of assumptions were made. These include assuming that the ball valve is an infinitely-long tube. The rest of assumptions are listed in Section 6.1.

Through the assumption of the valve being a tube, the stresses experienced by said cylinder can be related to the radius and thickness of the cylinder, as shown in Section 6.2. There are three stress components (axial, hoop and radial stress), and through analysis of their respective equations it was shown that the hoop stress is the most critical stress - hence it is this stress component that determines the minimum thickness of the valve body (assumed to be a tube). This means that with the hoop stress equation, one may calculate the required thickness for a chosen (yield) stress (and a constant tube radius).

In the process of weight optimization, it was decided to use the ”Ashby Material Selection” method to both select mechanically-appropriate materials for the valve body, and to finish optimizing the weight of said component. This method is described in detail in Section 6.3, and the results of this procedure is a selection of 4 different alloys, each with a different performance parameter (which quantifies the performance of said material type as the stress-to-density ratio). These alloys - from lowest to highest performance parameter - are listed below.

- Steel alloys
- Nickel alloys
- Aluminium alloys
- Titanium alloys

With these 4 alloys selected, their respective yield strengths can be obtained and used as input on the equations presented prior, which results in 4 different thicknesses - one per material. With said thicknesses (and assuming the tube is of the same length as the actual ball valve) the approximate weight of each valve can be calculated. Further assumptions of cost per kg for each material will also result in an approximate cost for each valve body depending on the material they are made of. All of this information is presented in Table D.2.

From this analysis, it would seem that the most reasonable material to use in the manufacture of the valve body would be the titanium alloy, due to its high performance parameter - which results in a remarkably low mass. However, due to the self-igniting risk of both the titanium and aluminium alloys, it was decided that the best (remaining) material candidate is the nickel alloy. This alloy allows the valve body to have a low mass, while keeping the material costs moderately low.

To close out the chapter, the method by which the weight of the valve body was verified using static structural analysis, whereby 4 different CAD models of the valve body (integrated with the rest of the valve components) were subjected to operational conditions, and their maximum stress values recorded to be compared with the yield strength of each one of the alloys selected. The results, compiled in Table 6.1, show that the results obtained through analysis were close to the expected stresses, with a maximum error of +11.4%, and an average error of 5.4%.

The results of this chapter are a methodology by which the weight of a ball valve body (usually its largest component) can be optimized, and a Python script - presented in Appendix C - that relates cylinder thickness (and hence valve body thickness) to the stress the cylinder experiences under a specific pressure.

7

Valve Redesign & Analysis

The initial design of the cryogenic ball valve that is the subject of the research (here-on referred to as the 'baseline' design) is a first iteration of a ball valve design. This iteration was not specifically designed for cryogenic service, nor optimized in any way.

As a result of these shortcomings, during testing of this first valve iteration, several problems arose. Without delving too much into detail, it was determined that several features of the current baseline ball valve had to be changed in order to improve its performance when subjected to cryogenic conditions. Furthermore, as to be in compliance with requirement **BV.4**, the baseline ball valve design had to be mass optimized.

With these points in mind, it was decided to re-design the cryogenic ball valve, parting from its baseline design, and using as input the designs of past rocket engine ball valves, as well as the findings from Chapter 6.

The purpose of this chapter is to document the valve re-design process, the steps taken to analyse the final valve iteration, and the results from said analysis.

The chapter is structured as follows. Section 7.1 documents the re-design process of the baseline cryogenic ball valve. Section 7.2 covers the entire set-up for the various simulations that were carried out in order to verify the new valve design. Section 7.3 presents the results of the different analyses set-up and described in the section prior. Finally, Section 7.4 which compiles the procedures presented throughout the chapter and concludes it.

7.1. Valve Redesign

This section presents the re-design process, parting from the original baseline ball valve design.

7.1.1. Baseline Valve Design

During the initial approach to the redesign problem, an initial baseline design of the cryogenic ball valve was provided. This design can be seen below, in full view in Figure D.1 and a cross section of this design in Figure D.2.

There are multiple features to note in this design. The first and most prominent of these is the floating ball design - the ball is actuated by the primary (and only) stem. This means in practice the ball has some freedom of movement in the longitudinal direction (parallel to fluid fow).

The second feature to note is the two-seat configuration, whereby the seats remain in place with no actuation whatsoever. The baseline design is neither a DBB or a DIB design - it is not able to relieve pressure from the cavity formed between the ball and the valve body.

It is worthy to note that this design is a 2-piece ball valve design, where the flange is attached to the valve body and limits the ball's movement. This type of design is simple to assemble and minimizes the number of joints (and hence O-rings) required, especially when compared to more complex 3-piece designs.

One last thing to note in this design is the lack of weight optimization throughout the valve body. Thick walls can be spotted in the ball housing region, as well as the downstream section of the valve. This adds a significant amount of weight, while providing no structural support whatsoever. This specific issue was addressed throughout Chapter 6, where weight optimization was discussed.

7.1.2. Redesigned Valve

Prior to the redesign process of the baseline ball valve, the conditions of operation of the ball valve were revised, along with the findings of the research on the multiple rocket ball valves found during the literature research, documented in Section 2.4.

When analyzing the valves presented in the literature research chapter, there are some common features and themes which can be spotted. The first of these features can be seen in the MOV and the MFV of the RS-25 engine, the gas generator ball valves of the F-1 engine, the oxidizer and fuel pump inlet valves of the RL10 engine, as well as possibly the MOV and the MFV of the LE-7 engine. All of these valves have a trunnion configuration. Although the reason for this is not known, it is believed that a trunnion valve may be able to achieve a better sealing, and lower operational torques.

The second feature present in many of these valves is the use of springs or bellows to press the valve seats into the ball. More precisely, both the MOV and the MFV of the RS-25 engine, the gas generator ball valves of the F-1 engine, and the oxidizer and fuel pump inlet valves of the RL10 engine all have some sort of mechanism by which the seat(s) are pressed unto the ball.

Throughout Chapter 6, a procedure for optimisation of the weight of the baseline ball valve design was presented. The results of this procedure, discussed in Section 6.4, can be implemented into this redesign, as the inner diameter of the valve body and the dimensions of the ball remain the same as the baseline design's. Along the same vein, the target of this redesign was to make the ball valve as compact as possible, taking inspiration from the oxidizer and fuel pump inlet valves of the RL10 engine by shortening the valve significantly.

The result of this redesign process is the valve presented below with a full view in Figure D.3 and a cross section in Figure D.4. To keep the redesign process simple, only specific components were redesigned. As a result, many of the components present in the baseline design are also present in the redesign. These include components such as bolts, washers, seats and seat supports. 4 different variations of this valve were made - each with a different valve body, whereby each valve body has a different thickness which corresponds to the thicknesses calculated in Section 6.4. This is discussed further later on in this chapter.

With this new valve re-design, the verification process of the new design can proceed - the set-up of which is discussed in the next section.

7.2. Analysis Set-Up

The findings presented in Section 6.4 include a set of optimal thicknesses, each corresponding to a different material out of the 4 material candidates selected prior. These thicknesses have been found through the usage of the yield strength of said materials. In order to verify the thicknesses calculated, as well as verify the new valve design, a set of analyses were carried out on different CAD models of the new cryogenic valve design. This section documents the boundary conditions imposed on the final iteration of the redesigned cryogenic ball valve, as documented in Section 7.1.

The first step in the verification process of the new valve design is to implement the optimal thicknesses

into separate CAD models - which can then be imported into analysis software. Since the weight optimization procedure only regarded the heaviest component (the valve body) the optimal thicknesses will only be imposed to said component in CAD, leaving all other components unchanged (effectively the same between CAD models).

As a result of this, 4 separate CAD models were generated, one per material type. The valve body CAD models of each are shown below, in Figure D.5, Figure D.6, Figure D.7 and Figure D.8, which are the steel, nickel, aluminium and titanium alloy valve bodies respectively. In these figures, it can be observed that overall the design barely changes between valve bodies - the only difference being the thickness of the ball housing.

These four valve bodies are then exported from the CAD software - integrated with the rest of the valve's components - as .STP files. Once these files were imported into ANSYS Workbench, 8 separate structural analysis cases were made - two cases per valve. The reason for this is that the valves will be working in cryogenic conditions - therefore it was decided to first set-up a Steady-State Thermal analysis case, followed by a Static Structural case. In the former, the temperature boundary conditions are applied, while in the later all other pressures/displacements/forces are applied, while using the results from the Steady-State Thermal case as input.

All valve assemblies were subjected to the same operating conditions, with the same analysis set-up for both the Steady-State Thermal and Static Structural cases. The imposed conditions on the valves are listed below.

- Proof pressure as specified in **BV.7**.
- Ball valve temperature of -180 ºC.
- No displacement of the downstream end of the ball valve body.
- Pre-tension of x N per bolt on the valve body - flange interface.

These can be visualized in the figures below.

Figure D.9, Figure D.10 and Figure D.11 present the static structural analysis case conditions - pressure, displacement and bolt pre-tension. On the other hand, Figure D.12 and Figure D.13 show the steady state thermal analysis case conditions - the cryogenic temperature assigned to the inside of the ball valve. For both cases, it is assumed that the LOX is occupying the entire ball housing (as well as the upstream section of the valve) - hence conditions such as pressure or temperature are assigned to surfaces within the ball housing, as well as the ball itself. It is assumed that the rest of the valve is at room temperature.

Along with the 4 different valves analysed, a 5th set of analyses was done on the baseline ball valve (the original valve, prior to re-design). This was done to ensure the validity of the other 4 structural analysis cases of the optimized valves. The analysis set-up is identical to that of the other 4 valves, therefore it will not be discussed further.

7.3. Results

The purpose of this section is to conclude this chapter, by presenting the results of the analyses as described in Section 7.2.

7.3.1. Steady-State Thermal Analyses

The first case that was run was the Steady-State Thermal analysis case for all of the valve variations. In these analysis cases, the only condition imposed on the valves were the cryogenic temperatures on faces in contact with LOX (as specified in Section 7.2). Running these thermal cases resulted in the same identical result, which is shown below in Figure D.14.

As shown in the figure, subjecting the upstream section of the ball valve(s) to a cryogenic temperature will eventually result in the entire ball valve reaching the same temperature, cryogenic conditions. This was the case for all of the valves, irrespective of the thickness of the valve body.

7.3.2. Static Structural Analyses

The first cases that were ran after setting up the analyses were the Static Structural cases. The results of these analyses were then used to verify the findings presented in Section 6.4. The verification of the weight optimization is documented in Section 6.5. The results of this first set of analyses is shown in Figure D.15, Figure D.16, Figure D.17 and Figure D.18 which are the results of analyzing the steel, nickel, aluminium and titanium alloy valve bodies (integrated with the rest of the valve components).

These figures show the locations of the peak stress within the valve body, as well as the value of said peak. Although (as discussed in Section 6.5) the peak stresses on some of these structural cases is slightly above the yield strength of their respective materials, this effect can be mitigated by adding a 20% safety margin on the originally-calculated thickness. Apart from this, the rest of the valve components behaved as expected - except for some unusual peak stresses most likely caused by improper meshing.

7.3.3. Steady-State Thermal & Static Structural Combined Analyses

Once the static structural analyses were carried out, the results from the steady-state thermal cases (discussed in Section 7.3.1) were used as input into new static structural analyses, for all four valve variants. The results of this are discussed below.

Figure D.19, Figure D.20, Figure D.21 and Figure D.22 show the peak stress locations and magnitudes for the steel, nickel, aluminium and titanium alloy valve bodies respectively. These results can be compared to the ones obtained in the subsection prior.

For the steel alloy valve body, the peak stress experienced by the valve increased significantly (by about 2.5%). Similarly, the titanium alloy valve body also experiences an increase in the peak stress, of about 4.9%. This is solely attributed to the effects of cryogenic conditions on the valve body material.

In contrast to the last two valves, the valve bodies for both nickel and aluminium alloys experience a decrease in peak stress, especially with the nickel alloy valve body. The aluminium alloy valve body has a decrease in peak stress of about 1.7%, while the nickel alloy valve body experienced a decrease in peak stress of 68.9%, by far the largest change out of the 4 valve bodies. Once again, these changes in peak stress are attributed to the addition of the cryogenic temperature input.

Taking the presented results into consideration, along with the findings in Section 6.4, it is clear that the most optimal material alloy for the valve body is the nickel alloy. The ball valve with the nickel alloy valve body performed best in all of the analyses carried out, whereby the peak stresses recorded in both static structural cases did not exceed the yield stress of the nickel alloy selected.

7.4. Conclusions

Throughout this chapter the re-design and analysis processes have been thoroughly documented, presenting the results.

In Section 7.1 the baseline design of the cryogenic ball valve is presented, analyzing its features and flaws. The flight heritage ball valves found during literature research are also analyzed, and the most prominent features from each are then used as input for the re-design process. Furthermore, the weight optimization results from Section 6.4 are also used as input to further minimize the weight of the re-design cryogenic ball valve. During this process, 4 separate valve bodies are made - one for each valve body material candidate.

Section 7.2 documents the process of setting-up the different analyses cases to verify the new cryogenic ball valve design. These consisted of two different types of analyses for each one of the 4 ball valve variants - a steady-state thermal analysis, and a static structural analysis. In the former, cryogenic conditions were imposed on the valve, while the latter analysis included all other operating conditions such as pressure, bolt pre-tension, and displacement.

Finally, Section 7.3 presents the results from all the analysis cases considered. This includes a steady-state thermal case, a static structural case, and a second static structural case which uses the steady-state thermal results as input. The results from the static structural case were used to verify the findings of the weight optimization procedure (as described in Section 6.5). There was a significant difference in the peak stresses observed in the valve body when taking into account the cryogenic temperatures - 2 of the alloys considered suffered an increase in peak stress (steel and titanium), while the other 2 alloys experienced a significant decrease in peak stress (nickel and aluminium). As a result, it is determined that the nickel alloy is the most suitable for the valve body within the redesigned ball valve.

8

Conclusions & Recommendations

At the beginning of this document, in Chapter 3, the following research objective was presented.

- The research objective is to design, iterate and analyse a cryogenic ball valve.

This research objective is of a broad nature. In order to break down the problem 6 relevant research questions were formulated, each broken down further into two research subquestions. The goal of the research phase of this project is to answer all of these questions.

The purpose of this chapter is to summarize the technical contents of this document, presenting the findings of each chapter, along with the answers to all of the formulated research questions.

The chapter is organized as follows. Section 8.1 discusses the torque models presented in Chapter 4. Section 8.2 discusses the flow factor model from Chapter 5. Next is Section 8.3, which summarizes the weight optimization methodology documented in Chapter 6. Section 8.4 discusses the valve redesign and analysis process from Chapter 7. Finally, Section 8.5 which presents the conclusions of other research questions not explicitly answered by the previous four chapters.

8.1. Torque Estimation Model

The purpose of this chapter was to investigate, implement and validate different torque estimation methods found during the literature research phase. This section briefly summarizes the procedures followed, and presents results.

First, the two different torque models found were introduced. The first, 'Model 1', was taken from the Aerospace Fluid Component Designer's Handbook [21], and consists of two torque component equations. In the document, it is claimed that this estimation method is suitable for trunnion ball valves. This model is exceptionally simple to implement.

The second model, 'Model 2', is a combination from the torque components presented in 'Air-Operated Valve Evaluation Guide' [20], along with the torque components presented in 'The Optimisation of the Floating Ball Valve Seat Component Design Methodology' [18]. Once combined, this model consists of 5 different torque components which depend on a multitude of variables - which in turn are able to estimate the opening and closing torque values for both trunnion and floating ball valves.

Both torque models were presented, and implemented into a single Python script (included in Appendix A). During the initial test of said script, it was noticed that the estimated torque values for both models were heavily dependent on the friction coefficients chosen. Due to this, it was decided to carry out a sensitivity analysis on all of the torque components that depend on any friction coefficient. From this analysis, it was found that nearly all of the torque components (except for the Hydrodynamic torque component) are directly proportional to their respective friction coefficients. Notably, τ_S and T_{DS} are

the torque components that are the most sensible to any change in friction coefficients (for Model 1 & Model 2 respectively).

Following the completion of the sensitivity analysis, it was decided to carry out a validation procedure on both torque estimation models. To do this, readily-available data gathered by the Testing team was used. This data was gathered for ball valves with known geometry at different pressures - this includes torque data - which was then compared to the torque estimation values generated by both Model 1 and Model 2. The resulting table shows the accuracy of both models at estimating the required torque.

Table 8.1: Error of both models used to estimate torque values, compared to experimental data.

	Floating Configuration				**Trunnion Configuration**			
Pressure (bar)	50	70	90	108	50	70	90	108
Model 1 Error (%)	-	-	-	-	-	-	1.211	-4.888
Model 2 Error (%)	-0.359	-8.409	-0.005	-5.844	-	-	11.681	9.002

Table 8.1 shows that Model 1 seems to be more accurate in its torque estimation values (with errors of less than $\pm$5%. When it comes to estimating the torque for the floating ball valve, Model 2 has an error of less than $\pm$8.5%, while for the trunnion ball valve the Model 2 error increases up to $\pm$11.7%.

During this chapter, the following research questions (from Chapter 3) were answered.

- **RQ3:** How much torque is required to operate a ball valve?
  - **RQ3.a:** How can a ball valve's operational torque be modelled?
  - **RQ3.b:** How can a ball valve's torque model be validated?

RQ3.a was answered through the presentation of the two torque estimation models (as discussed above), while **RQ3.b** was answered in the validation section of Chapter 4 - by using torque data gathered by the Testing team and comparing it directly to torque data obtained from the two torque estimation models.

From the results of this chapter, it is recommended to study the validity of both models further, using a larger array of experimentally-gathered torque data, with a wider pressure range, and also including different valve sizes with varying geometries. It is also recommended to look into the option of using machine learning as a way to predict torque values, by feeding a model experimental data along with valve data, and having torque as an output of said machine learning model.

8.2. Flow Factor Model

The objective of Chapter 5 was to present a method by which the flow factor (K_v) of an opening ball valve can be estimated. This section presents the methodology followed and the results obtained.

The flow factor is a value which helps in indicating how 'efficient' a component is at passing fluid through. This value depends on a multitude of variables, which are either calculated or approximated throughout this chapter.

The first value addressed is that of the geometric opening area of a ball valve - as flow rate directly depends on this area, and flow rate is one of the variables needed to calculate K_v. In order to calculate this value, it was assumed that the opening area of a ball valve at any given value is equal to the intersection area of two circles assumed of equal diameter. One circle represents the ball bore, and the other circle represents the valve bore. This method was then implemented into a Python script - shown in Appendix B. The result of this script is a set of plots of opening area vs. ball rotation, such as the one shown in Figure 8.1.

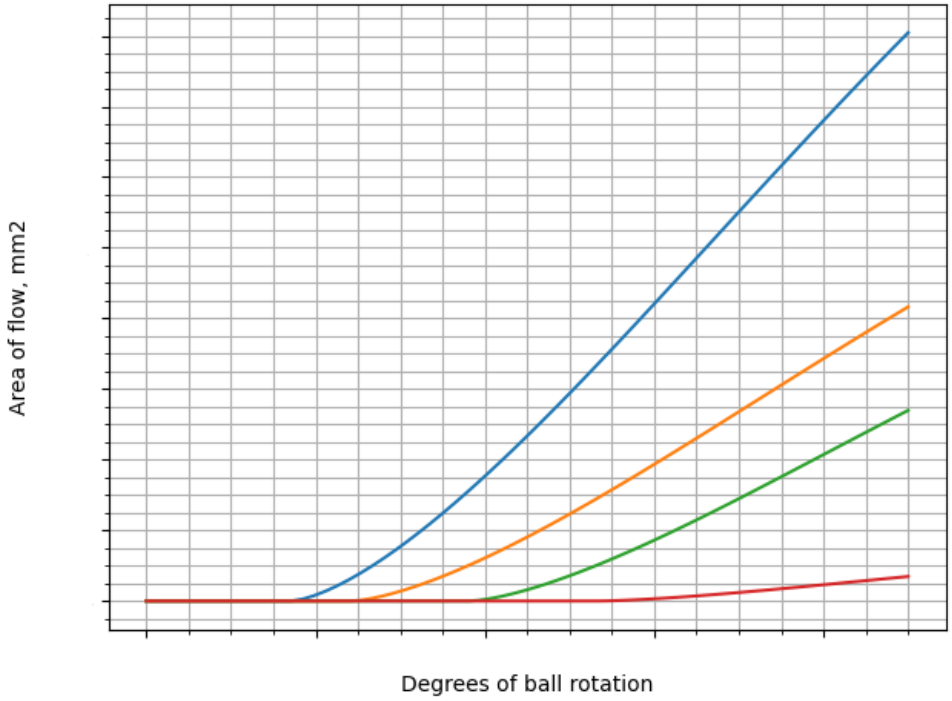

Figure 8.1: Area of flow vs. ball rotation for different ball valve sizes.

In order to verify the validity of the aforementioned area calculations, a set of verification procedures were carried out. These include hand calculations, comparison with areas from a valve's CAD model, and comparison with opening area data from two available valves.

The next step in the flow factor calculation process is approximating the pressure loss across the ball valve as it opens. For this procedure, it was decided to use experimental data gathered by the Testing team in order to approximate a relation between pressure loss and ball rotation. This was then combined with the geometric opening area calculations, to obtain the flow factor distribution of a ball valve as it opens. An example plot of the K_v values of two different ball valves is shown below, in Figure 8.2. This figure showcases the effect of using the estimated pressure loss distribution, versus assuming a constant pressure loss (which results in a K_v distribution similar to the geometric opening area profile).

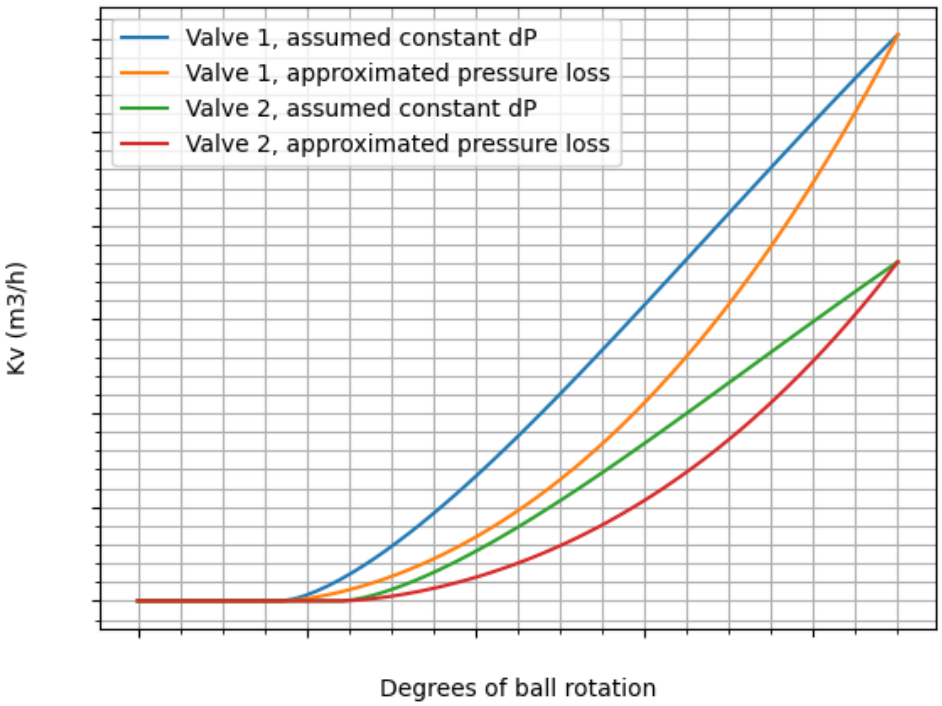

Figure 8.2: Flow factor (K_v) versus degrees of ball rotation, for 2 different valves. Each valve has 2 lines - one where a constant pressure loss is assumed (hence the profile of this line resembles that of the opening area distribution), and one with an approximated pressure loss as the valve opens (taken from experimental measurements).

The goal of this chapter was to answer the following research question (which is broken down into two subquestions) as formulated in Chapter 3.

- **RQ2:** How does fluid flow change as the ball valve is operated?
  - **RQ2.a:** How does opening area change as the ball valve is operated?
  - **RQ2.b:** How does flow factor change as the ball valve is operated?

RQ2.a was answered throughout Section 5.1, whereby the geometric opening area of a ball valve was calculated and presented in figures such as Figure 8.1. The change in opening area depends on the geometrical properties of the ball valve being considered, as well as the initial angle at which there is any opening at all. Figure 8.1 itself shows the geometric opening area of multiple valve sizes.

RQ2.b was addressed by implementing the findings of the previous research subquestion, and by estimating a pressure loss distribution as the ball valve opens. Both of these factors were implemented into a Python script which can in turn display the flow factor plotted against the degrees of ball rotation of a ball valve. The relation of flow factor versus degrees of ball rotation is similar to that of the opening area versus the ball rotation, although adding an increasing pressure loss as the ball rotation is reduced significantly decreases the magnitude of the calculated flow factor, as shown in Figure 8.2.

Based on the findings of this chapter, it is recommended to further inquire into methodologies by which the pressure loss across a ball valve can be calculated. More accurate pressure loss values as the ball valve is opened will in turn result in more accurate flow factor estimations.

8.3. Valve Weight Optimization

During this chapter, a procedure by which ball valves can have their mass minimized is proposed. This procedure only considers the heaviest component of a ball valve - the valve body.

Several assumptions are made in order to simplify the problem. One of the key assumptions is as-

suming the valve is an infinitely-long tube. Another important assumption is that this tube is thick-walled.

Using the radial, hoop and axial stress equations for such a tube, a plot was made to determine which one of the stress components constraints the thickness of the tube. The minimum required thickness vs. the allowable stress was plotted for all three stress components, and it was found that for this specific problem the critical stress component is that of the hoop stress, σ_{hoop}.

To optimize the weight of the valve (and select material candidates) the Ashby Material Selection method was used. In this method, a specific performance parameter is formulated (based on the component geometry and the hoop stress equation) which when maximized will result in the lowest component weight. The performance parameter for this specific problem is $\frac{\sigma_{hoop}}{\rho}$. This line was plotted on an Ashby graph, where it was used to select four different alloys. These are the following:

- Steel alloys
- Nickel alloys
- Aluminium alloys
- Titanium alloys

With the material alloys selected, the thicknesses required for each material can now be calculated. This is done using the hoop stress formula presented earlier in the chapter.

The final material chosen for the valve body was the nickel alloy, as the other better-performing alloys (titanium and aluminium) are not to be used with cryogenic flow, due to the risks of self-ignition [35].

To verify the 4 different thickness values calculated, a valve body was made for each material, with their corresponding thickness. These valves were all subjected to operational conditions, and their peak stresses were recorded and compared to the yield stresses of each one of the materials. The error between these two values does not exceed $\pm$11.4%. From these results, it is recommended to add a 20% margin to the thickness values obtained, in order to avoid peak stresses within the valve body from reaching the yield stress of the material used.

During this chapter, the following research questions were answered.

- **RQ1:** How can a ball valve be optimized for weight?
  - **RQ1.a:** Which ball valve components can be mass-optimized?
  - **RQ1.b:** How can the structure of a mass-optimized ball valve be verified?

The approach to answer **RQ1.a** was to consider the ball valve components which could be mass-optimized in the most straightforward manner. For this reason, it was chosen to focus on the valve body of the ball valve, which is commonly the heaviest component out of the entire valve. To tackle this problem, it was assumed that the geometry of the valve body could be approximated to an infinitely-long tube.

Answering **RQ1.b** required the use of static structural analysis of the valve, after implementing new thicknesses to the valve bodies generated (one per material candidate). The analysis was set up to recreate the operational conditions the valve will experience (with the same pressure as the pressure used as input during the weight optimization process). The peak stresses within the valve body were recorded, and compared to the yield stresses of the materials selected for the valve body.

8.4. Valve Redesign & Analysis

The purpose of this chapter was to present the methodology followed to redesign the baseline cryogenic ball valve design, and the analysis done in order to verify this new design.

The first step in the redesign was to document the baseline design, with its current design features.

This was followed by a small description of some of the observations on the ball valves found during the literature research, in Section 2.4. Along with this, the findings of Chapter 6 were also implemented in the redesign, in the interest of keeping the mass of the new ball valve design as low as possible.

The result of this process is a new ball valve design which implements features common in similar cryogenic ball valves from past rocket engine systems, with a minimized valve body weight.

For the purpose of verification of the redesigned ball valve, a set of analyses were set up for the 4 different ball valve CAD models - one per material candidate, as per the conclusions in Chapter 6. These 4 ball valve models were subjected to three analysis cases: a steady-state thermal analysis, a static structural analysis, and a second static structural analysis where the results from the steady-state thermal analysis were used as input. This allowed for insight into the effects of cryogenic conditions on the mechanical performance of the new ball valve design, for each one of the 4 material alloy candidates.

The conclusions of this chapter are that due to cryogenic conditions, the ball valves made out of the steel alloy and the titanium alloy both experienced increases in peak stress values of 2.5% and 4.9% respectively. In contrast, the nickel and the aluminium alloy ball valves experienced a reduction in the peak stress values of 1.7% and 68.9% respectively. Based on this analysis (and the conclusions of Chapter 6) it is clear that the most optimal material candidate for the redesigned valve is the nickel alloy.

By the end of this chapter, the following research questions have been answered.

- **RQ4:** How can the current ball valve design be improved?
  - **RQ4.a:** What ball valve elements are required for this specific application?
  - **RQ4.b:** How can said elements be incorporated into the current design?

RQ4.a is centered around the features required for a cryogenic ball valve. As shown during Chapter 7, there are several features that similar valves share. These features include:

- A trunnion ball valve configuration
- A spring/bellows to exert force upon the valve seat(s)
- An overall compact design

These features can be beneficial if a valve is operating in cryogenic conditions, hence their implementation into the new design of the ball valve.

RQ4.b was answered throughout Section 7.1.2, where the redesigned ball valve was compared to the baseline design as presented in Section 7.1.1. The implementation of a more compact design was directly influenced by the design of the Oxidizer & Fuel Pump Inlet ball valves from the RL10 engines.

From the work done in this chapter, there are several recommendations for future work of the design of the valve. First, there should be some design work to assess how requirements **BV.10** and **BV.11** can be implemented into the current ball valve design, as this was not done during the re-design process. It is also recommended to reconsider the design of the secondary shaft of the ball valve, especially its interface with the valve body. Another recommendation is to carry out further analysis into the specific components used in the valve re-design, and determine whether they are apt to the re-designed valve body (this includes aspects such as material compatibility).

8.5. Cryogenic Conditions & Future Ball Valves

Throughout the technical section of this document, there are two topics which are not addressed directly; the effects of cryogenic conditions on a ball valve, and the extrapolation of the results in this document to future valves. These issues, although implicitly answered, will now be explained more thoroughly.

Research question 5, which deals with the issue of cryogenyc temperatures, is listed below, along with its respective subquestions.

- **RQ5:** What effects does cryogenic conditions impose on the operation of a ball valve?
  - **RQ5.a:** How do cryogenic conditions affect mechanical properties of the ball valve's components?
  - **RQ5.b:** How do cryogenic conditions affect surface properties of the ball valve's components?

The first subquestion (**RQ5.a**) is answered in Chapter 7, when comparing the static structural analysis cases with the other static structural analysis cases that use the steady-state thermal results as inputs. A non-significant change in the peak stresses experienced by the valve body is seen. As a general rule, as the temperature of a metal decreases, its mechanical properties increase [15]. This is partially corroborated by some of the findings in Chapter 7, where it was found that under cryogenic conditions the nickel alloy and aluminium alloy valve bodies performed better than at room temperature conditions. For unknown reasons, this was not the case with the steel and titanium alloy valve bodies.

The second subquestion, **RQ5.b**, concerns the effects of cryogenic temperatures on the surface properties of ball valve components. For the most part, this should not be of concern to the operation of a ball valve, as unlike with changes in mechanical properties, a variation in surface properties of the materials that make up the ball valve's components should not change its operation. This is indeed the case with most of the aspects of a ball valve considered in this document - flow factor calculations, weight optimization, and the different structural analyses - except for torque estimation.

As mentioned during Chapter 4, both torque estimation models are directly proportional to the chosen friction coefficient values. These friction coefficient values (such as the seal friction coefficient μ_S of the seal friction torque component of model 1) depend on the materials of the two components in contact (in this case, the seat and the ball). Friction coefficient values have been known to vary with temperature. Teflon is a widely used material in ball valve seats, due to its notably low friction. In cryogenic temperatures, the friction coefficient of Teflon tends to increase significantly[30]. An increase of friction coefficient directly implies an increase in the values of almost all torque components for both torque estimation models. These variations in surface properties must be taken into account when selecting friction coefficient values for cryogenic versus non-cryogenic ball valves.

The last research question to be addressed is that of considerations of the findings of this document in other (future) ball valves. This question, along with its respective subquestions, is presented below.

- **RQ6:** How can the conclusions & findings be extrapolated to other ball valves?
  - **RQ6.a:** How do operational conditions differ in other ball valves within the system?
  - **RQ6.b:** What design changes could be implemented as to adapt the current ball valve design to said operational conditions?

RQ6.a is a question that considers the system in which the designed ball valve may operate. The ball valve considered in this document - with its requirements as listed in Section 2.1) - operates at the highest pressure experienced in the system (which is specified in **BV.6** & **BV.7**). Furthermore, this ball valve operates under cryogenic conditions - which may not be the case for all the required valves within the relevant system.

Considering valves with different (and most likely lower) pressures will definitively affect all of the considered aspects of a ball valve (torque, flow factor, weight optimization and design). Both the torque estimation models and the weight optimization procedure depend on operating pressure alone, without the need of other estimations. Because of this, the scripts generated from the torque and weight optimization models can be directly used with other pressures as inputs.

This however is not the case for the flow factor estimation model, as an approximated pressure loss distribution (based on experimental data) is used to fully estimate the flow factor across the ball valve.

A way to circumvent this issue would be to have a preliminary pressure loss distribution based on the operating pressure of the valve in question, and on the pressure loss of a straight pipe of internal dimensions equivalent to those of the valve in question.

The other research subquestion, **RQ6.b**, regards the applicability of design features of the redesigned ball valve to other ball valves operating in dissimilar conditions. With respect to valves operating at lower pressures, the ball valve may require an adjustment in the spring/bellow properties (possibly to reduce the force that this component exerts on the valve seat) as to not increase the operating torque. If the operating pressure of the valve is too low, the floating ball configuration could be investigated, as it is a lighter alternative to the trunnion configuration, but its torque values do not scale well with increasing pressure. Other design features such as the valve body thickness may be changed by using the new operating pressure as input.

If the ball valve type is switched from trunnion to floating, it is also recommended to reconsider the usage of spring/bellow components to exert force on the seats altogether. This is especially the case in ball valves that work in non-cryogenic conditions, as the fluid will not be as susceptible to evaporate - hence the pressures accumulated in the ball housing (the volume entrapped by the valve body and the ball) will not be as high. This removes the necessity of the DIB or DBB systems (which was discussed in Section 2.3.7).

References

[1] ACI. *Ball valves*. 2024. URL: https://www.aci24.com/en/help-center/fittings-help-center/what-is-a-ball-valve.html (visited on 03/22/2024).

[2] National Aeronautics and Space Administration. *Liquid Rocket Valve Assemblies*. Tech. rep. Lewis Research Center, 1973.

[3] National Aeronautics and Space Administration. *Liquid Rocket Valve Components*. Tech. rep. Lewis Research Center, 1973.

[4] Daniel Osezua Aikhuele. *Design, Manufacture and Simulation of ball valves for oil industrial applications*. Master's thesis. May 2011.

[5] Valve World Americas. *Introduction to Ball Valves*. 2022. URL: https://valve-world-americas.com/introduction-to-ball-valves/ (visited on 04/11/2020).

[6] R. R. Atherton. *Advanced Cryogenic Rocket Engine Program Staged-Combustion Concept*. Tech. rep. Pratt & Whitney Aircraft, 1967.

[7] BBD. *Seat with delta ring*. 2024. URL: http://www.bbdsrl.it/valves-seats-and-components/components-for-ball-valves/seats-for-side-entry-valves/seat-with-delta-ring/?lang=en (visited on 03/22/2024).

[8] Oscar Biblarz and Edward W. Price. *Development of rockets*. 2024. URL: https://www.britannica.com/technology/rocket-jet-propulsion-device-and-vehicle/Development-of-rockets (visited on 09/17/2024).

[9] Robert E. Biggs. *SPACE SHUTTLE MAIN ENGINE THE FIRST 10 YEAR - Part 7 – Main Oxidizer Valve Fire, Main Fuel Valve Fracture, Nozzle Feed Line Failures*. 1992. URL: https://www.enginehistory.org/Rockets/SSME/SSME7.pdf (visited on 04/04/2024).

[10] Cameron International Corporation. *Cross Section of a Ball Valve*. 2024. URL: https://www.wermac.org/images_large/valve_ball.html (visited on 03/22/2024).

[11] IMI CRITICAL. *Top Entry Ball Valves*. 2024. URL: https://www.imi-critical.com/product/top-entry-ball-valves/ (visited on 03/22/2024).

[12] J. P. B. Cuffe. *Design Study of RL10 Derivatives*. Vol. 2nd volume. NASA, 1974.

[13] Design and Engineering. *Ball Valve Design Features*. 2020. URL: https://designandengg.com/ball-valve-design-features/ (visited on 03/26/2024).

[14] Granta Design. *Material Property Charts*. 2020. URL: https://www.grantadesign.com/education/students/charts/ (visited on 08/29/2024).

[15] P. Duthil. *Material Properties at Low Temperature*. URL: https://cds.cern.ch/record/1973682/files/arXiv:1501.07100.pdf.

[16] Eric Eberly. *Area of Intersecting Circles*. 2009. URL: https://www.engineeringtoolbox.com/area-intersecting-circles-d_1571.html (visited on 08/29/2024).

[17] Yukio Fukushima et al. "DEVELOPMENT STATUS OF LE-7A AND LE-5B ENGINES FOR H-IIA FAMILY". In: *Acta Astronautica* 50.5 (2002), pp. 275–284. ISSN: 0094-5765. DOI: https://doi.org/10.1016/S0094-5765(01)00165-5. URL: https://www.sciencedirect.com/science/article/pii/S0094576501001655.

[18] Nicholas Gray. *The Optimisation of the Floating Ball Valve Seat Component Design Methodology*. Master's thesis. July 2019.

[19] Parker Hannifin. *Actuation and System Design and Evaluation - OMS Engine Shutoff Valve*. Tech. rep. National Aeronautics and Space Administration, 1975.

[20] J. Hosler. *Air-Operated Valve Evaluation Guide*. Final Report. 3412 Hillview Avenue, Palo Alto, California: EPRI, 1999.

[21] Glen W. Howell and Terry M. Weathers. *Aerospace Fluid Componen Designers' Handbook*. Revision D. Redondo Beach, California: NASA, 1970.

[22] RFS HYDRAULICS. *3 Piece Full Bore 1000 PSI Stainless Steel Threaded / Socket Weld End Ball Valve*. 2024. URL: https://www.rfshydraulics.com/3-piece-ball-valve.html (visited on 03/22/2024).

[23] Lauren□iu-Ioan Ivancu and Daniela Popescu. "Investigation of the Fluid Flow in a Large Ball Valve Designed for Natural Gas Pipelines". In: *Applied Sciences* 13.7 (2023), p. 4247. DOI: https://doi.org/10.3390/app13074247.

[24] Steve Jurvetson. *Lunar Module Ascent Engine Valve Package Assembly*. 2010. URL: https://www.flickr.com/photos/jurvetson/4886815765 (visited on 03/22/2024).

[25] K. Katsuta, H. Miyajima, and K. Suzuki. *Development Status of LE-7 H-II Rocket Main Engine*. AIAA, 1986. URL: https://arc-aiaa-org.tudelft.idm.oclc.org/doi/pdf/10.2514/6.1986-1409.

[26] Charles Kolstad. *V-Port Ball Valves and Their Uses*. 2022. URL: https://tameson.com/pages/v-port-ball-valve (visited on 03/22/2024).

[27] T. Leephakpreeda. "Design factors for "linear" ball valve: theoretical and experimental studies". In: *ThaiScience* 27.2 (2005), pp. 353–361.

[28] Zhen-hao Lin et al. "Fluid dynamic analysis of liquefied natural gas flow through a cryogenic ball valve in liquefied natural gas receiving stations". In: *Energy* 226 (2021). Cited by: 15. DOI: 10.1016/j.energy.2021.120376. URL: https://www.scopus.com/inward/record.uri?eid=2-s2.0-85103082684&doi=10.1016%2fj.energy.2021.120376&partnerID=40&md5=b78f2a86cce3be2848f150364727d6ce.

[29] GLOBAL SUPPLY LINE. *DBB, DIB-1 and DIB-2 Ball Valves*. 2011. URL: https://globalsupplyline.com.au/wp-content/uploads/2021/03/DBBvsDIB.pdf (visited on 03/22/2024).

[30] N. L. McCook et al. "Cryogenic Friction Behavior of PTFE based Solid Lubricant Composites". In: *Tribology Letters* 20 (2005), pp. 109–113. DOI: https://doi.org/10.1007/s11249-005-8300-4.

[31] Kimble D. McCutcheon. *Rocketdyne F-1 Engine Description*. 2022. URL: https://www.enginehistory.org/Rockets/RPE08.11/RPE08.12.shtml (visited on 03/22/2024).

[32] Kimble D. McCutcheon. *The Lunar Module Ascent Engine (LMAE)*. 2022. URL: https://www.enginehistory.org/Rockets/RPE09.44/RPE09.44.shtml (visited on 03/22/2024).

[33] Kimble D. McCutcheon. *The Pratt & Whitney RL10 Engine*. 2023. URL: https://www.enginehistory.org/Rockets/RPE08.21/RPE08.21.shtml (visited on 03/22/2024).

[34] NASA. *Block IIA - SSME Propellant Flow Schematic*. 2015. URL: https://pbs.twimg.com/media/CL2pTAAUYAAuQGf?format=jpg&name=900x900 (visited on 04/02/2020).

[35] S. Peralta, Keisa R. Rosales, and Joel M. Stoltzf. "Liquid Oxygen Rotating Friction Ignition Testing of Aluminum and Titanium with Monel® and Inconel® for Rocket Engine Propulsion System Contamination Investigation". In: *ASTM International* (2009). URL: https://ntrs.nasa.gov/api/citations/20090006758/downloads/20090006758.pdf.

[36] Inc. Safe Water Technologies. *Specific Gravity of Common Liquids and Fluids*. URL: https://www.swtwater.com/catalog/pdf/Specific-Gravity-of-Common-Liquids.pdf (visited on 10/24/2024).

[37] Rainer Schnell, Jonas Klingwort, and James Farrow. "Locational privacy-preserving distance computations with intersecting sets of randomly labeled grid points". In: *International Journal of Health Geographics* 20 (Mar. 2021). DOI: 10.1186/s12942-021-00268-y.

[38] Dr. Duane Shelton and Dr. George Gamota. *Space And Transatmospheric Propulsion Technology*. Tech. rep. NASA / JTEC, 1990. URL: https://ntrs.nasa.gov/api/citations/19910007821/downloads/19910007821.pdf.

[39] Zhiyong Shu et al. “Transient flow dynamics behaviors during quick shut-off of ball valves in liquid hydrogen pipelines and storage systems”. In: *Journal of Energy Storage* 73 (Dec. 2023), p. 109049. DOI: 10.1016/j.est.2023.109049.

[40] Jess Sia. *Rocket Physics*. 2021. URL: https://www.marssociety.ca/2021/03/25/rocket-fuel/ (visited on 09/17/2024).

[41] Aircraft Engine Historical Society. *The SM Serice Propulsion System (SPS)*. 2024. URL: https://www.enginehistory.org/Rockets/RPE09.30/RPE09.31.shtml (visited on 03/24/2024).

[42] Spaceaholic. *Artifact: Rocket Engine, RS-18, Valve Package Assembly (VPA), Lunar Module (LM) Ascent Stage*. 2014. URL: http://www.spaceaholic.com/index.php/Detail/Object/Show/object_id/25# (visited on 04/02/2020).

[43] George P. Sutton and Oscar Biblarz. *Rocket Propulsion Elements*. 9th ed. Wiley, 2017.

[44] Tameson. *2-Way Manual Ball Valve – Basic Principles*. 2018. URL: https://www.engineeringclicks.com/2-way-ball-valve-basic-principles/ (visited on 03/22/2024).

[45] The Engineering ToolBox. *Stress in Thick-Walled Cylinders or Tubes*. 2005. URL: https://www.engineeringtoolbox.com/stress-thick-walled-tube-d_949.html (visited on 09/18/2024).

[46] DBV Valve. *Valve Types with Their Advantages and Disadvantages*. 2021. URL: https://dbaovalve.com/valve-types/ (visited on 04/18/2024).

[47] H. Wichmann. *OMS Engine Shutoff Valve and Actuation System Design and Evaluation*. Tech. rep. The Marquardt Company, 1974.

A

Torque Estimation Models Code

Note: All values presented in this code are non-confidential, and only for the purpose of presenting sample values to be used in the presented functions.

```
import numpy as np
import matplotlib.pyplot as plt

def BearingTorqueModel1(DP, miu_B, d_p):        # Output in in-lb
    return 1.75*10**-3 * DP**(3/2) * d_p**4 * miu_B

def SealingTorqueModel1(DP, miu_S, d_p):        # Output in in-lb
    return 0.625 * DP * d_p**3 * miu_S

def StaticSeatTorque(d_MS, DP, v, E, d_B, miu_S, F_spring):         # Output in in-lb
    b = np.pi * d_MS
    F_PL = DP * np.pi * d_MS**2 / 4
    alpha = np.arcsin(d_MS/d_B)
    F_SS = F_PL * np.cos(alpha)
    P_1 = F_SS / (np.pi * d_MS)
    E_star = 1 / ((1-v**2) / E)
    a_1 = ((4*((d_B*25.4)/2)*P_1*0.175126835)/(np.pi*E_star))**(1/3) /25.4
    P_01 = P_1 / (np.pi * a_1)
    P_ls = 1.05 * DP
    w = F_spring/(np.pi*d_MS)
    a_2 = ((4*(d_B*25.4/2)*w*0.175126835)/(np.pi*E_star))**(1/3) /25.4
    P_e = w / (np.pi*a_2)
    P_3 = P_1 + w
    a_3 = ((4*(d_B*25.4/2)*P_3*0.175126835)/(np.pi*E_star))**(1/3) /25.4
    P_03 = P_3 / (np.pi*a_3)
    if P_03 >= P_ls:
        print("Valve will seal successfully")
    else:
        print("Valve will not seal")
    return 2 * miu_S * P_e * 2 * a_2 * b * ((d_B)**2 - (d_MS/2)**2)**0.5

def PackingLoadTorque(DP, d_S, h_P, miu_P):         # Output in ft-lb
    G_stress = 1500         # Alternatively, G_stress = 1.5*DP
    F_PL = G_stress * 0.5 * np.pi * d_S * h_P * miu_P
    return F_PL * d_S / 2 / 12

def DynamicSeatTorque(DP, d_MS, d_B, miu_S):        # Output in ft-lb
    return ((DP * np.pi/4 * d_MS**2 * d_B)/((d_B**2 - d_MS**2)**0.5)) * (miu_S) * ((d_B + (
        d_B**2 - d_MS**2)**0.5)/(48))

def BearingTorque(DP, d_MS, miu_B, d_S):            # Output in ft-lb
    return DP * np.pi/4 * d_MS**2 * miu_B * d_S/24

def HydrodynamicTorque(DP, d_p, Q_MAX, rho):        # Output in ft-lb
    Ksys = ((894.01 * d_p**4 * DP)/(Q_MAX**2)) * (62.4/rho)
    print("The Ksys value is ", Ksys, "\n")
```

```
    # HTF = float(input("Please input value of HTF, according to the calculated Ksys value:
        "))
    HTF = (177.25/(Ksys + 15.4924))**(1/1.32569)        # Approximated Ksys - HTF relation
    # print(HTF)
    return 1/12 * DP * (HTF/100) * d_p**3

########## INPUTS ##########
DP = 50 / 10                                    # Nmm-2
v = 0.46                                        # -
E = 600                                         # N mm-2
d_MS =  60                                      # mm
d_B =   80                                      # mm
d_S =   15                                      # mm
d_p =   40                                      # mm
h_P = 30                                        # mm
Q_MAX = 1                                       # kg/s
rho =   1000                                    # kg/m3
miu_S = 0.05                                    # -
miu_B = 0.4                                     # -
miu_P = 0.2                                     # -
F_spring = 210.002                              # lb

########## CONVERSION ##########
DP = DP * 145.037738                            # PSI
d_MS = d_MS / 25.4                              # inch
d_B = d_B / 25.4                                # inch
d_S = d_S / 25.4                                # inch
d_p = d_p / 25.4                                # inch
h_P = h_P / 25.4                                # inch
Q_MAX = Q_MAX * 1/rho * 1/0.00378541 * 60       # gpm
rho = rho * 0.062428                            # lb/ft3


######### CALCULATIONS ##########
# All torque values converted from imperial units to Nm
T_SS = StaticSeatTorque(d_MS, DP, v, E, d_B, miu_S, F_spring) * 1.3558179483/12
T_DS = DynamicSeatTorque(DP, d_MS, d_B, miu_S) * 1.3558179483
T_B = BearingTorque(DP, d_MS, miu_B, d_S) * 1.3558179483
T_H = HydrodynamicTorque(DP, d_p, Q_MAX, rho) * 1.3558179483
T_P = PackingLoadTorque(DP, d_S, h_P, miu_P) * 1.3558179483
T_B1 = BearingTorqueModel1(DP, 0.3, d_p) * 1.3558179483/12
T_S = SealingTorqueModel1(DP, 0.3, d_p) * 1.3558179483/12

########## RESULTS ##########
print("MODEL 1 TORQUE RESULTS:")
print("Ball Valve Torque Required, in Nm: ", T_B1 + T_S, "\n")
print("MODEL 2 TORQUE RESULTS:")
print("Total Floating Ball Valve Opening, in Nm: ", T_P + T_SS + T_DS + T_H)
print("Total Floating Ball Valve Closing, in Nm: ", T_P + T_SS + T_DS)
print("Total Trunnion Ball Valve Opening, in Nm: ", T_P + T_SS + T_B + T_H)
print("Total Trunnion Ball Valve Closing, in Nm: ", T_P + T_SS + T_B)
```

B

Geometric Area & Flow Factor Code

Note: All values presented in this code are non-confidential, and only for the purpose of presenting sample values to be used in the presented functions.

```
import matplotlib.pyplot as plt
import numpy as np

def Area(r, r_out, t):
    r = r / 2000
    r_out = r_out / 2000
    d = 2*r
    x = np.linspace(0,d,int(100*t+1))
    theta = 2*np.arccos((r-x/2)/r)*180/np.pi
    A= r**2*(np.pi/180*theta-np.sin(theta*np.pi/180))
    A = np.append([0], A)
    gamma = (np.arccos((x**2 / (-2*r_out**2)) + 1) * 180/np.pi) + ((np.arccos(r/r_out)-np.
        arcsin(r/r_out))*180/np.pi)
    gamma = np.append([0], gamma)
    return A, gamma

def MassFlow(r, mdot, rho, Area):
    A = np.pi*(r/2000)**2
    v = mdot / (rho * A)
    return Area*rho*v

def Kv(Q, SG, dP):
    return Q*(SG/dP)**0.5

def mdottoQ(mdot, rho):
    return (1/rho)*mdot*3600

def pressdistro(x):
    return (3.770044*np.exp((-0.026731*x)))

# from CAD
Valve1 = {'BallID': 50, 'BallOD': 80, 'SeatID': 52, 'SetOD': 57, 'mdot': 45, 'rho': 1141, 'SG
    ': 1.14}
Valve2 = {'BallID': 30, 'BallOD': 65, 'SeatID': 40, 'SetOD': 44, 'mdot': 27, 'rho': 774, 'SG'
    : 0.82}
Valve3 = {'BallID': 10, 'BallOD': 28, 'SeatID': 13, 'SetOD': 14, 'mdot': '???', 'rho': 1141,
    'SG': 1.14}
Valve4 = {'BallID': 30, 'BallOD': 60, 'SeatID': 35, 'SetOD': 47, 'mdot': '???', 'rho': 1141,
    'SG': 1.14}
Valve5 = {'BallID': 27, 'BallOD': 50, 'SeatID': 33, 'SetOD': 40, 'mdot': '???', 'rho': 774, '
    SG': 0.82}
Valve6 = {'BallID': 32, 'BallOD': 48, 'SeatID': '???', 'SetOD': '???', 'mdot': '???', 'rho':
    1141, 'SG': 1.14}
Valve7 = {'BallID': 22, 'BallOD': 42, 'SeatID': '???', 'SetOD': '???', 'mdot': '???', 'rho':
    774, 'SG': 0.82}

```

```
A_Valve1, gamma_Valve1 = Area(Valve1['BallID'], Valve1['BallOD'], 0.5)
A_Valve2, gamma_Valve2 = Area(Valve2['BallID'], Valve2['BallOD'], 0.5)
A_Valve3, gamma_Valve3 = Area(Valve3['BallID'], Valve3['BallOD'], 0.5)
A_Valve4, gamma_Valve4 = Area(Valve4['BallID'], Valve4['BallOD'], 0.5)
A_Valve5, gamma_Valve5 = Area(Valve5['BallID'], Valve5['BallOD'], 0.5)
A_Valve6, gamma_Valve6 = Area(Valve6['BallID'], Valve6['BallOD'], 0.5)
A_Valve7, gamma_Valve7 = Area(Valve7['BallID'], Valve7['BallOD'], 0.5)


############################## PLOTTING ##############################

plt.figure(1)
plt.plot(gamma_Valve1, A_Valve1*10**6, label = "Calculated␣Valve␣1")
plt.plot(gamma_Valve2, A_Valve2*10**6, label = "Calculated␣Valve␣2")
plt.plot(gamma_Valve3, A_Valve3*10**6, label = "Calculated␣Valve␣3")
plt.plot(gamma_Valve4, A_Valve4*10**6, label = "Calculated␣Valve␣4")
plt.plot(gamma_Valve5, A_Valve5*10**6, label = "Calculated␣Valve␣5")
plt.xlabel("Degrees␣of␣ball␣rotation")
plt.ylabel("Area␣of␣flow,␣mm2")
plt.grid()
plt.grid(which = "minor")
plt.minorticks_on()
plt.legend()

plt.figure(2)
plt.plot(gamma_Valve1, MassFlow(Valve1['BallID'], Valve1['mdot'], Valve1['rho'], A_Valve1))
plt.xlabel("Degrees␣of␣ball␣rotation")
plt.ylabel("Mass␣flow,␣kg/s")
plt.grid()

plt.figure(3)
#plt.plot(gamma_Valve1*100/90, A_Valve1*10**6, label = "Calculated Valve 1")
#plt.plot(gamma_Valve2*100/90, A_Valve2*10**6, label = "Calculated Valve 2")
#plt.plot(gamma_Valve5*100/90, A_Valve5*10**6, label = "Calculated Valve 5")
#plt.plot(gamma_Valve3*100/90, A_Valve3*10**6, label = "Calculated Valve 3")
plt.plot(gamma_Valve6*100/90, A_Valve6*10**6, label = "Calculated␣Valve␣6")
plt.plot(gamma_Valve7*100/90, A_Valve7*10**6, label = "Calculated␣Valve␣7")
plt.xlabel("%␣of␣ball␣rotation")
plt.ylabel("Area␣of␣flow,␣mm2")
plt.grid()
plt.legend()

vfunc = np.vectorize(pressdistro)
result = vfunc(gamma_Valve1)
plt.figure(4)
plt.plot(gamma_Valve1, Kv(mdottoQ(MassFlow(Valve1['BallID'], Valve1['mdot'], Valve1['rho'],
    A_Valve1), Valve1['rho']), Valve1['SG'], 0.34), label = 'Valve␣1,␣Assumed␣constant␣dP␣=␣
    0.34␣bar')
plt.plot(gamma_Valve1, Kv(mdottoQ(MassFlow(Valve1['BallID'], Valve1['mdot'], Valve1['rho'],
    A_Valve1), Valve1['rho']), Valve1['SG'], result), label = 'Valve␣1,␣Approximated␣pressure
    ␣loss')
plt.plot(gamma_Valve2, Kv(mdottoQ(MassFlow(Valve2['BallID'], Valve2['mdot'], Valve2['rho'],
    A_Valve2), Valve2['rho']), Valve2['SG'], 0.34), label = 'Valve␣2,␣Assumed␣constant␣dP␣=␣
    0.34␣bar')
plt.plot(gamma_Valve2, Kv(mdottoQ(MassFlow(Valve2['BallID'], Valve2['mdot'], Valve2['rho'],
    A_Valve2), Valve2['rho']), Valve2['SG'], result), label = 'Valve␣2,␣Approximated␣pressure
    ␣loss')
plt.xlabel("Degrees␣of␣ball␣rotation")
plt.ylabel("Kv␣(m3/h)")
plt.grid()
plt.grid(which = "minor")
plt.minorticks_on()
plt.legend()
plt.show()
```

C

Weight Optimization Thickness Code

Note: All values presented in this code are non-confidential, and only for the purpose of presenting sample values to be used in the presented functions.

```
import matplotlib.pyplot as plt
import numpy as np

# INPUTS
P_in = 5.0                      # Pa
R_in = 50.8                     # mm
t_max = 7
P_out = 0
t = np.linspace(0, 7, 100)

# CALCULATIONS
sigma_axial = (P_in*R_in**2 - P_out*(t+R_in)**2)/((t+R_in)**2 - R_in**2)
sigma_hoop = ((P_in*R_in**2 - P_out*(t + R_in)**2)/((t+R_in)**2 - R_in**2)) - ((R_in**2 * (t+
    R_in)**2 * (P_out - P_in))/(R_in**2 * ((t+R_in)**2 - R_in**2)))
#sigma_radi = ((P_in*R_in**2 - P_out*(t + R_in)**2)/((t+R_in)**2 - R_in**2)) + ((R_in**2 * (t
    +R_in)**2 * (P_out - P_in))/(R_in**2 * ((t+R_in)**2 - R_in**2)))
t_radi = (P_in*R_in**2 - P_in*(t+R_in)**2) / ((t+R_in)**2 - R_in**2)
sigma_radi = np.linspace(0, 1400, 100)
for i in range(0, 100):
    t_radi[i] = 0

# PLOTTING
plt.plot(sigma_axial, t, label = "Axial Stress")
plt.plot(sigma_hoop, t, label = "Hoop Stress")
plt.plot(sigma_radi, t_radi, label = "Radial Stress")
plt.axis(xmin = 0, xmax = 1400, ymin = -1, ymax = 7)
plt.xlabel("Allowable Stress (MPa)")
plt.ylabel("Minimum Thickness (mm)")
plt.legend()
plt.grid()
plt.show()
```